Defense Threat Reduction Agency
8725 John J. Kingman Road, MS
6201 Fort Belvoir, VA 22060-6201

DTRA-TR-10-69

TECHNICAL REPORT

Solid State Recrystallization of Single Crystal Ce:LSO Scintillator Crystals for High Resolution Detectors

June 2012

HDTRA1-07-1-0001

David W. Snyder and
Charles R. Shanta

Prepared by:
Pennsylvania State Electro-Optics Center
559A Freeport Rd.
Freeport, PA 16229

DESTRUCTION NOTICE:

Destroy this report when it is no longer needed.
Do not return to sender.

PLEASE NOTIFY THE DEFENSE THREAT REDUCTION AGENCY, ATTN: DTRIAC OP-ONIU, 8725 JOHN J. KINGMAN ROAD, MS-6201, FT BELVOIR, VA 22060-6201, IF YOUR ADDRESS IS INCORRECT, IF YOU WISH THAT IT BE DELETED FROM THE DISTRIBUTION LIST, OR IF THE ADDRESSEE IS NO LONGER EMPLOYED BY YOUR ORGANIZATION.

CONVERSION TABLE

Conversion Factors for U.S. Customary to metric (SI) units of measurement.

MULTIPLY →	BY →	TO GET
TO GET ←	BY ←	DIVIDE
angstrom	1.000 000 x E -10	meters (m)
atmosphere (normal)	1.013 25 x E +2	kilo pascal (kPa)
bar	1.000 000 x E +2	kilo pascal (kPa)
barn	1.000 000 x E -28	meter^2 (m^2)
British thermal unit (thermochemical)	1.054 350 x E +3	joule (J)
calorie (thermochemical)	4.184 000	joule (J)
cal (thermochemical/cm^2)	4.184 000 x E -2	mega joule/m^2 (MJ/m^2)
curie	3.700 000 x E +1	*giga bacquerel (GBq)
degree (angle)	1.745 329 x E -2	radian (rad)
degree Fahrenheit	$t_k = (t°f + 459.67)/1.8$	degree kelvin (K)
electron volt	1.602 19 x E -19	joule (J)
erg	1.000 000 x E -7	joule (J)
erg/second	1.000 000 x E -7	watt (W)
foot	3.048 000 x E -1	meter (m)
foot-pound-force	1.355 818	joule (J)
gallon (U.S. liquid)	3.785 412 x E -3	meter^3 (m^3)
inch	2.540 000 x E -2	meter (m)
jerk	1.000 000 x E +9	joule (J)
joule/kilogram (J/kg) radiation dose absorbed	1.000 000	Gray (Gy)
kilotons	4.183	terajoules
kip (1000 lbf)	4.448 222 x E +3	newton (N)
kip/inch^2 (ksi)	6.894 757 x E +3	kilo pascal (kPa)
ktap	1.000 000 x E +2	newton-second/m^2 ($N-s/m^2$)
micron	1.000 000 x E -6	meter (m)
mil	2.540 000 x E -5	meter (m)
mile (international)	1.609 344 x E +3	meter (m)
ounce	2.834 952 x E -2	kilogram (kg)
pound-force (lbs avoirdupois)	4.448 222	newton (N)
pound-force inch	1.129 848 x E -1	newton-meter (N-m)
pound-force/inch	1.751 268 x E +2	newton/meter (N/m)
pound-force/foot^2	4.788 026 x E -2	kilo pascal (kPa)
pound-force/inch^2 (psi)	6.894 757	kilo pascal (kPa)
pound-mass (lbm avoirdupois)	4.535 924 x E -1	kilogram (kg)
pound-mass-foot^2 (moment of inertia)	4.214 011 x E -2	kilogram-meter^2 ($kg-m^2$)
pound-mass/foot^3	1.601 846 x E +1	kilogram-meter^3 (kg/m^3)
rad (radiation dose absorbed)	1.000 000 x E -2	**Gray (Gy)
roentgen	2.579 760 x E -4	coulomb/kilogram (C/kg)
shake	1.000 000 x E -8	second (s)
slug	1.459 390 x E +1	kilogram (kg)
torr (mm Hg, 0^0 C)	1.333 22 x E -1	kilo pascal (kPa)

*The bacquerel (Bq) is the SI unit of radioactivity; 1 Bq = 1 event/s.

**The Gray (GY) is the SI unit of absorbed radiation.

REPORT DOCUMENTATION PAGE

Form Approved
OMB No. 0704-0188

PLEASE DO NOT RETURN YOUR FORM TO THE ABOVE ORGANIZATION.

1. REPORT DATE *(DD-MM-YYYY)*	2. REPORT TYPE	3. DATES COVERED *(From - To)*
12-01-2010	Final Technical Report	Nov 2006- July 2009

4. TITLE AND SUBTITLE
Solid State Recrystallization of Single Crystal Ce:LSO Scintillator Crystals for High Resolution Detectors

5a. CONTRACT NUMBER

5b. GRANT NUMBER
HDTRA1-07-1-0001

5c. PROGRAM ELEMENT NUMBER

6. AUTHOR(S)
Snyder, David, W
Shanta, Charles, R

5d. PROJECT NUMBER

5e. TASK NUMBER

5f. WORK UNIT NUMBER

7. PERFORMING ORGANIZATION NAME(S) AND ADDRESS(ES)
Pennsylvania State Electro-Optics Center
559A Freeport Rd
Freeport PA 16229

8. PERFORMING ORGANIZATION REPORT NUMBER

9. SPONSORING/MONITORING AGENCY NAME(S) AND ADDRESS(ES)
DTRA-R&D Enterprise
8725 John J. Kingman Rd
Ft. Belvoir, VA 22060

10. SPONSOR/MONITOR'S ACRONYM(S)
DTRA

11. SPONSOR/MONITOR'S REPORT NUMBER(S)

12. DISTRIBUTION/AVAILABILITY STATEMENT

13. SUPPLEMENTARY NOTES

14. ABSTRACT

Ce:Lu2SiO5 crystals were produced by solid state recrystallization (SSR). In this process an energetically metastable polycrystalline material is placed in contact with a single crystal seed. Upon thermal processing the primary grain grows due to the reduction in interfacial energy of the grain boundaries in the polycrystalline material. This study examined SSR of undoped Lu2SiO5 over temperatures range 1400°C – 1900°C at times up to 50 hours. The recrystallization rate was negligible below 1700°C and was only 0.28 microns/hr at 1750°C. The effect of adding up to 2% CaO and up to 2% MgO was studied over the same temperature range. At 1750°C, MgO doping at 2% was observed to increase the SSR rate of the primary crystal to 40 microns/hr while CaO doping at 2% increased the SSR rate of the primary crystal to 20 microns/hr. CaO doping was observed to have an insignificant increase in grain size for the ceramic matrix. Samples up to 3mm thick were produced using this approach. Experimental results were fit to a parabolic rate equation for both the primary grain and the polycrystalline matrix.

15. SUBJECT TERMS
Ce:Lu2SiO5, solid state recrystallization, recrystallization kinetics, parabolic rate equation

16. SECURITY CLASSIFICATION OF:			17. LIMITATION OF ABSTRACT	18. NUMBER OF PAGES	19a. NAME OF RESPONSIBLE PERSON
a. REPORT	b. ABSTRACT	c. THIS PAGE			James Howell, James.Howell@dtra.mil
Unclassified	Unclassified	Unclassified	UU		19b. TELEPHONE NUMBER *(Include area code)* (703)767-2853

Introduction

Proliferation and/or use of weapons of mass destruction (WMD) are significant challenges to national security. The Defense Threat Reduction Agency (DTRA) Nuclear Detection Technology Research, Development, Test and Evaluation (RDT&E) Program (DTRA/NTD) develops portable, high resolution, highly efficient, and/or room temperature radiation detectors and sensors for a variety of applications in combating WMD. These system(s) will need to incorporate advances in nuclear detection materials.

This effort developed a fundamental understanding of nuclear and radiological detection material growth processes and operational mechanisms as a basis for advanced materials exploration and exploitation for maximum performance. Advances in our knowledge of scintillation and semiconductor materials, plastics, organics, glass, synthesized nano-crystal fabrics and fluids as well as crystalline materials; predictive models of detection performance; models of nuclear radiation interactions with solid state materials; nuclear detection crystal growth; knowledge of the dynamics of radiation detection processes; knowledge of optical transport and interactions in scintillation materials; and knowledge of the capabilities of nanostructured nanotubular, superconducting or other extremely innovative materials and their possible exploration in nuclear detection are all necessary to meeting the challenges of WMD proliferation and use.

Ceramics consist of small (~ 1's to 10's of μm in diameter), randomly oriented crystals (crystallites or grains) separated by grain boundaries. They are not used for gamma detectors, because the grain boundaries act as scattering sites that reduce light yield [1]. Instead gamma scintillators are single crystals solidified from a melt. There are no interior boundaries in crystals and therefore very few scattering sites [1]. Ceramics are produced in high volume resulting in low production costs per unit volume of yielded material. However, crystal growth is a much lower volume process (especially for oxides) with high production costs.

The rare earth oxides (including yttrium) are activated scintillators (as opposed to intrinsic scintillators such as BGO); that is, they need to be doped, usually with Ce^{3+}, in order to be an effective scintillator. The scintillation light in these materials is a result of 4f-5d transitions in the Ce^{3+} ion [2]. In the case of LSO the host lattice provides very few energy levels close to the Ce transitions. Therefore there are few electron traps leading to non-radioactive transitions that quench the primary scintillation mechanisms. In addition the host lattice has a high band gap limiting the creation of free electron-hole pairs during scintillation events. As a result a large amount of scintillation is due to Ce^{3+} excited states and excitons (bound electron-hole pairs) which decay very quickly [2].

Solid State Recrystallization (SSR) utilized low cost ceramic processing methods, with an additional step. By taking advantage of unique thermodynamic processes, SSR converts the ceramic to a single crystal. Liquid phase growth techniques such as the Czochralski process have severe limitations, specifically, maximum doping levels due to liquid solubility limits and uniformity due to dopant segregation. The key contribution of this work was to overcome these current issues by introduce higher levels of cerium doping, improved uniformity and reduced cost using the solid state recrystallization approach.

The ideal SSR process is to first produce a densified ceramic compact with submicron grain size. Then bond a single crystal seed to the compact and thermally cycle. During the thermal cycle the ceramic compact would be converted into a single crystal.

This project addressed area A. Radiological and Nuclear Detection Material Science, Research Concentration Area 3, Experimental and Theoretical Investigations of Nuclear Detection Crystal Growth.

Objective

The objective of the this project was to develop increased resolution, increased sensitivity low cost cerium-doped single crystal growth of Lu-based scintillators (Lu_2SiO_5:Ce (LSO)) using solid state recrystallization (SSR) of ceramic into single crystals.

By increasing the levels of cerium dopant in LSO scintillator crystals, advanced detector performance and detection capability will be obtained resulting in greater resolution and higher signal output and subsequently larger standoff, improved resolution detectors.

Executive Summary

Solid State Recrystallization of Ce:LSO has been demonstrated during this project and crystals up to 3mm thick were produced. In this study two approaches, internally and externally seeded, were evaluated. The concentration dependencies of two grain growth additives, calcium oxide (CaO) and magnesium oxide (MgO) were studied and kinetic rate models were developed for the primary crystal and the matrix grain growth. Finally, the effect of cerium concentration was evaluated.

In order to study the recrystallization kinetics an internal seeding method was developed in which a small seed crystal was embedded in ceramic perform which was then thermally processed at varying temperatures and times. While this method suffers from stress induced cracking due to the densification of the perform, it allows for efficient measurement of recrystallization kinetics for a wide range of experimental variables.

Recrystallization rates for pure (undoped) LSO were found to be extremely low. At a synthesis temperature of 1750°C the recrystallization rate was only 0.25 μ/hr and the resultant grain size ranged between 1-2 μm.

Recrystallization additives where evaluated found to dramatically increase the observed recrystallization rate. Up to 2% CaO and MgO was evaluated over the temperature range from 1400°C – 1900°C at times up to 50 hours. Growth rates increased by 125X with the addition of 2% MgO and 60X with the addition of 2% CaO. At 1750°C adding 2% CaO increased the recrystallization rate to 20 microns/hr and adding 2% MgO increased the recrystallization rate to 40 μ/hr. Although MgO-doped LSO showed the largest growth rate, CaO was found to be the preferred dopant for SSR since it was observed have little impact grain size for the polycrystalline matrix. For LSO processed at 1750°C for 50 hours, the CaO doped ceramic matrix grains size was 18 μm whereas the MgO doped grain size was 375 μm.

Experimental results were fit to a parabolic rate equation for both the primary grain and the polycrystalline matrix for undoped LSO, CaO doped, MgO doped and CeO doped LSO at levels up to 4% over a wide temperature range. The recrystallization kinetics were found to be well described by the parabolic rate equation.

Externally seeded experiments were evaluated at multiple temperature, time, and gas ambients. Fully densified polycrystalline compacts were prepared by uni-axial hot pressing for one hour at 10 MPa. Forming temperature for Ce:LSO was 1600°C for LSO and 1700°C. For undoped LSO externally seeding was not effective due to the slow growth rate which resulted in poor growth initiation.

Recommendations for future efforts focus on combining grain growth additives with an external seeding approach, a combination not considered during this project. In such an approach external seeding studies should focus on a three step process consisting of first forming polycrystalline CaO-doped LSO compacts by hot pressing followed by externally bonding the polycrystalline matrix to a single crystal seed in air and finally thermal processing in vacuum for recrystallization. The advantage in this approach is that it combines the rapid recrystallization due to the presence of CaO (essential for both seed attachement and growth) with low thermal expansion and densification induced stresses.

Technical Approach

Lu_2SiO_5 doped with cerium (Ce:LSO) has been identified as an extremely attractive scintillation crystal. Ce:LSO is of great interest due to it's superb light output (27000 photons/MeV), high density (7.4 g/cm3), short decay time (~ 40 ns) and appropriate emission wavelength (420 nm) [8]. One key application of Ce:LSO is gamma-ray detection.

Ce:LSO is typically grown by the Czochralski technique at temperatures near 2100 C. In addition to the high material growth cost, common is from the Czochralski process is, iridium inclusions, cracking and dopant variations [5]. Another key limitation is the low crystal-to-melt distribution coefficient of ~ 0.22 [8] which limits the amount of cerium that can be incorporated into the crystal and results in significant variations in cerium along the length of a boule thus limiting yield.

This project used a novel solid state recrystallization method to growth single-crystal Ce:LSO to produce large area, near-net-shape, high uniformity, highly doped crystals at temperatures up to 600°C lower than are currently used in Czochralski growth. We increased the cerium levels in the crystal by four times.

SSR process consists of conversion of a polycrystalline ceramic into single crystal by placing a seed crystal internal to the ceramic or by bonding a seed crystal to the ceramic surface and annealing in an appropriate atmosphere at an elevated temperature. The boundaries between the crystal grains in the ceramic have a high surface area and subsequently a high surface energy. The lower surface area of the seed crystal results in a thermodynamic driving force that promotes migration of the single crystal-polycrystal interface into the polycrystal matrix. At the elevated temperature, the migration of the boundary proceeds at a kinetically favorable rate resulting in growth of the single crystal region.

In order to enhance the boundary migration rate, it was necessary to add a material at the ceramic grain boundaries that becomes liquid at the elevated temperature. The presence of this liquid phase has been shown to significantly enhance the boundary migration.

In this program an SSR crystal growth was developed and the following issues have been investigated:

Task 1: Ceramic Preform Fabrication and Seed Attachment

Work on SSR of other oxide crystals clearly identified the need to develop a ceramic preform free of porosity and having a uniform composition and distribution of dopants. This project was focused on producing Ce:LSO ceramics using conventional powder processing. The experimental matrices were designed to optimize the process to maximize density of the ceramic. In addition the effect of temperature, gas atmosphere, pressure and time on the ceramic grain structure was documented.

The goal of this task was to produce a dense, small grain Ce:LSO ceramic preform. Issues that were investigated include:

- Powder processing
- Remilling to reduce particle size
- Compaction using one of three approaches: cold pressing/sintering (CPS), cold isostatic pressing and sintering, and uniaxial hot pressing (HP)

The task characterized density, grain size and studied seed attachment (external seeding). The seed attachment studied, included the evaluation of the effects of surface finish, force, temperature and time.

Powder processing and particle size reduction

The chemical source material selected for use in the solid state recrystallization of LSO is listed in figure 1.1. The source material was selected based on purity and particle size. In addition Lu_2SiO_5 was purchased from Nanocerox for comparison in particle size and surface area on the prepared material.

Chemical formula	Supplier	Purity
Lu_2O_3	Nanocerox	99.99
SiO_2	ProChem	99.99
Ce_2O_3	PIDC	99.99
Lu_2SiO_5	Nanocerox	99.99

Figure 1.1 chemical source material for LSO SSR experiments

Each source material was characterized for particle size by Malvern MasterSizer 2000. Gaussian particle size distribution (PSD) and X-ray diffraction (XRD) charts for lutetium oxide, silica, and lutetium silica oxide are located in figures 1.2 through 1.4 and average particle size is summarized in figure 1.5.

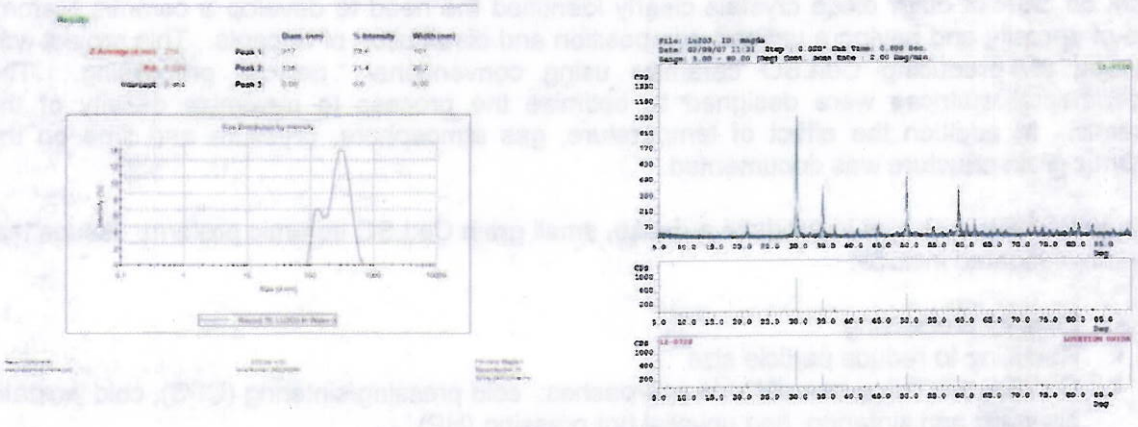

Figure 1.2, PSD and XRD data for lutetium oxide

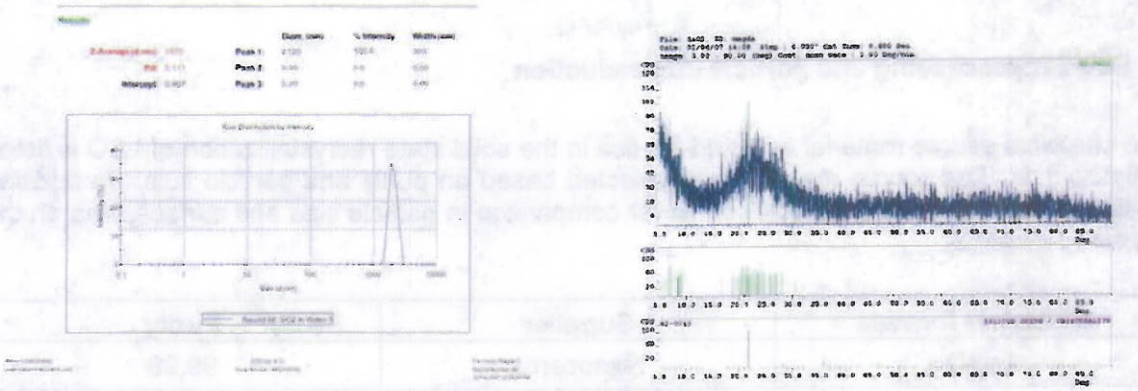

Figure 1.3, PSD and XRD data for silica

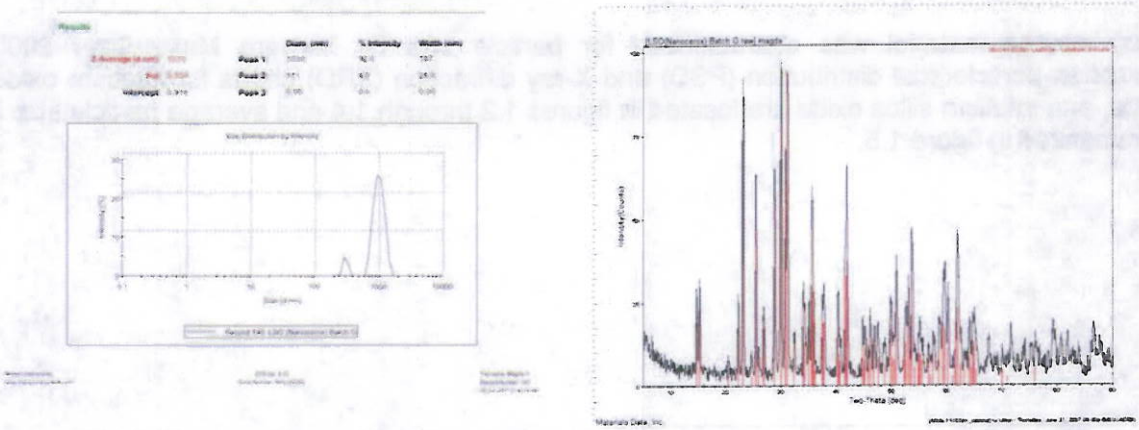

Figure 1.4, PSD and XRD data for lutetium silica oxide from Nanocerox, Batch G

Material	Average particle size (nm)
Lutetium oxide	274
Silica	1970
Cerium Oxide	1000
Nanocerox LSO	1070

Figure 1.5, Summary of average particle size distribution and surface area

The chemical composition of the mixture was fixed at the stoichiometric ratio. The source chemical powders were mixed in a HTPE bottle by 15 mm high purity Y-stabilized zirconia media for 24hr in ethanol. After milling, the solution was dried on a hot plate while magnetically stirred. The dried powder was calcined in an alumina crucible in air at 1200°C for two hours. After calcining, the powder was ball milled again to reduce the particle size. The material was then sieved to a particle size of 177μm in a standard three inch brass sieve. The average particle size was 620nm.

Cold Pressing and Sintering Ceramic Preform Fabrication

Cold Pressing and Sintering (CPS) Method

For the CPS experiments performed during this time period the following experimental parameters were held constant:

- Thermal ramp rates = 5°C/min
- Chamber pressure = 50 mTorr
- Gas ambient = nitrogen
- Cold press forming pressure= 100ksi

Experimental identification	Temperature (°C)	Dwell Time (hours)
TTI-LSO-01	1850	10
TTI-LSO-02	1850	5
TTI-LSO-03	1850	1
TTI-LSO-04	1750	10
TTI-LSO-05	1750	5
TTI-LSO-06	1750	1

Figure 1.6. Temperature and time used for initial CPS experiments for undoped LSO source.

The temperature-time effects were studied for four chemical compositions within each thermal cycle as summarized in figure 1.6.

Two major observations were made from this set of experiments:

- Low density (<99%) was observed for all conditions
- Density was observed to increase with increasing CeO_2

Multiple experiments were conducted by the CPS method; however, radial cracking of the green preform typically occurred after the extraction form the die. After sintering the preforms were found to split along the cracks as shown in Figure 1.7. Defects were believed to be the result of differential "spring back", which occurred during formation of the preform in the cold press process. "Spring back" can generally be induced by several effects:

- Friction with the die wall causing pressure gradients within the preform.
- Non-uniform granules, particles and die filling, resulting in elastic energy gradients.
- High radial pressures within the preform due to die restraint.

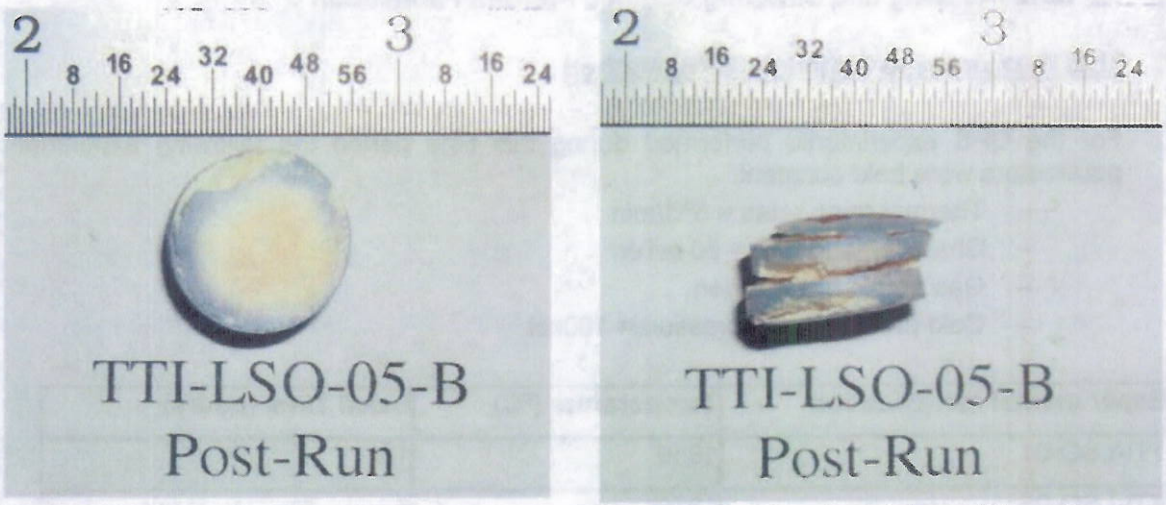

Figure 1.7. Typical LSO preform produced by CPS method. Experimental conditions: 5 press cycles at 690 MPa (100ksi), 1750°C for 5 hours in vacuum, standard scale.

The majority of effort on this subtask focused upon reducing pressure gradients, and radial pressures. Figure 1.8 shows a general pressure profile during a press cycle [15]. In our experiments, press cycling was used to reduce the pressure gradients within the green perform. Efforts for reducing the radial pressures included the use of extraction aids, force variation, and dwell times.

For the press cycling experiments the following parameter ranges were studied:

Number of cycles:	1, 2, 5 and 10
Force:	10MPa and 100MPa
Dwell time per cycle:	1, 2, and 5 minutes

None of the conditions were able to produce a crack free green preform with repeatability and all ceramic preforms produced via the CPS approach had cracks throughout.

Due to the issues with producing high quality, high density performs, comprehensive grain size analysis was not completed for the CPS samples. Preliminary estimates showed that the grains approached 100μm in size for 10 hr runs at both 1750°C and 1850°C

A summary of measured density for CPS samples is shown in Figure 1.9. Density was observed to increase with increasing cerium concentration and performs with the highest density contained 4% cerium for all temperature-time conditions. Figure 1.10 is a plot which illustrates the increase in density with increasing cerium concentration. Additional experiments will be conducted to understand the mechanism for this observation. Figure 1.11 shows macroscopic cracking and grain structure of TTI-LSO-01-B sintered at 1850°C for 10 hours.

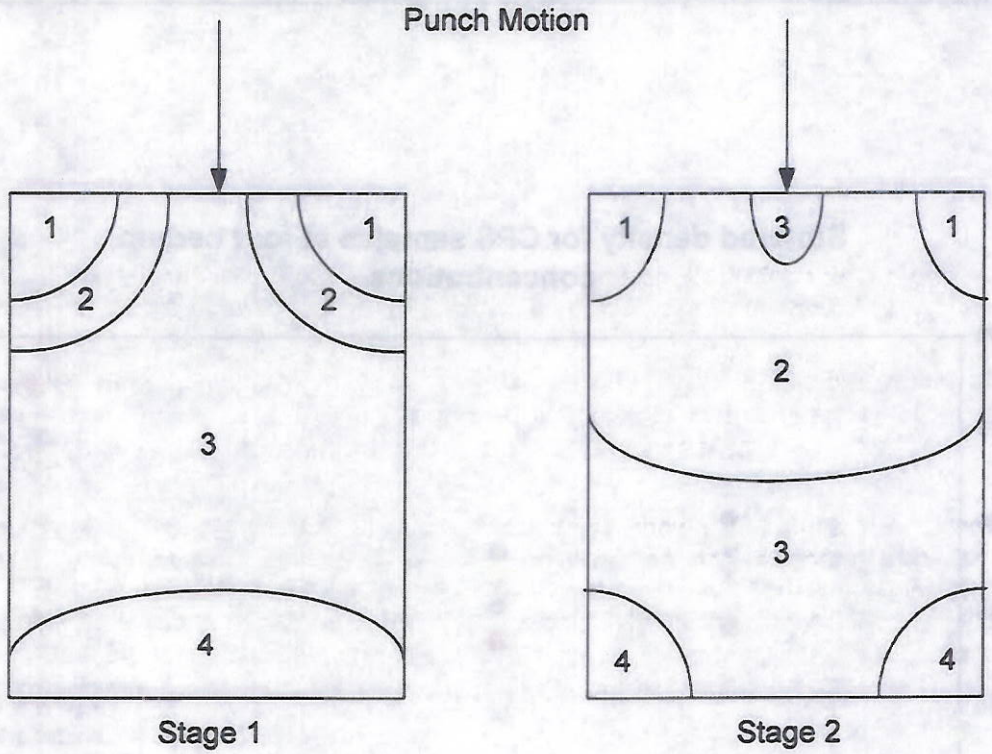

Figure 1.8. General pressure profile of uniaxial pressing[15]. Note radial and axial pressure gradients present near outer corners of samples.

Figure 1.9. Sintered density for CPS samples for four chemical compositions.						
Chemical composition	**TTI-LSO-01 1850C/10 hrs**	**TTI-LSO-02 1850C/5 hrs**	**TTI-LSO-03 1850C/1hr**	**TTI-LSO-04 1750C/10hrs**	**TTI-LSO-05 1750C/5hrs**	**TTI-LSO-06 1750C/1hr**
Lu_2SiO_5	6.35 (86%)	5.5 (74.3%)	5.82 (78.6%)	6.24 (84.4%)	6.39 (86.4%)	6.13 (82.9%)
Lu1.99Ce0.01SiO5	6.55 (88.6%)	6.24 (84.4%)	6.59 (89.1%)	6.23 (84.3%)	6.44 (87.1%)	6.67 (90.2%)
Lu1.98Ce0.02SiO5	6.32 (85.6%)	6.18 (83.6%)	6.47 (87.6%)	5.89 (79.7%)	6.38 (86.4%)	6.53 (88.4%)
Lu1.96Ce0.04SiO5	6.98 (94.7%)	7.17 (97.2%)	6.90 (93.6%)	6.97 (94.6%)	6.81 (92.4%)	6.25 (84.8%)

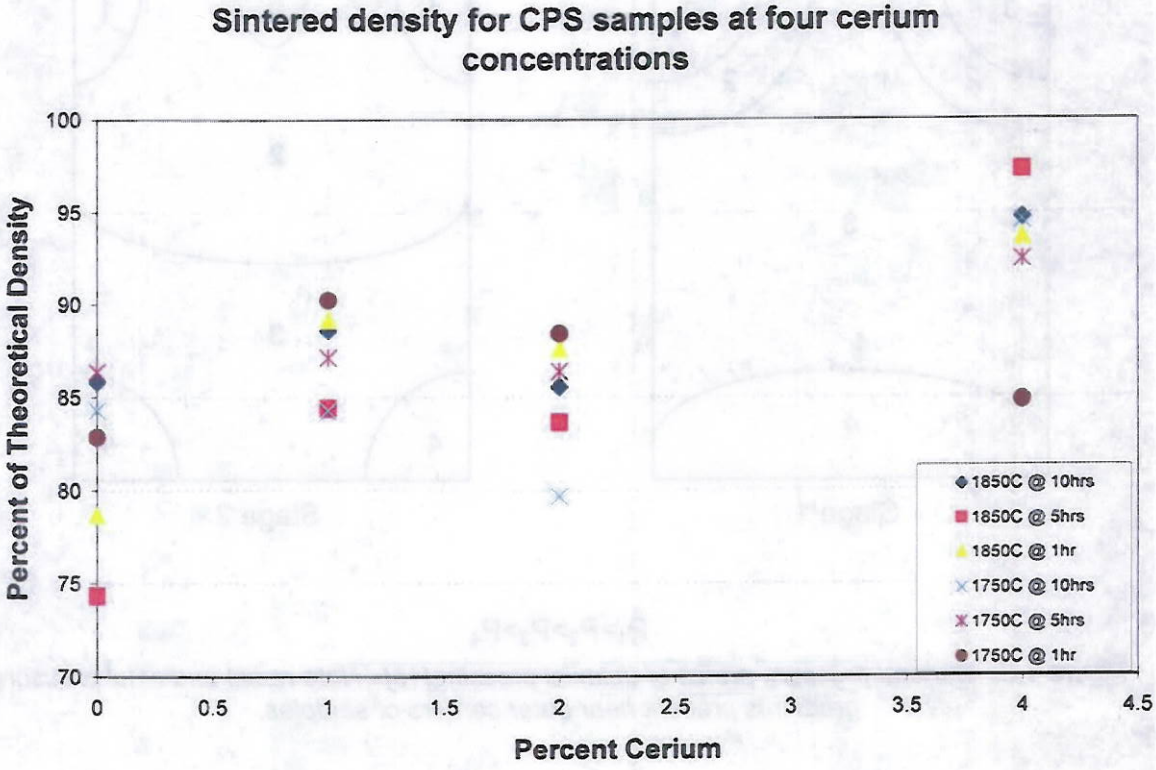

Figure 1.10. Comparison of measured density for CPS samples as a function of cerium concentration up to 4% showing density increase with increasing cerium doping .

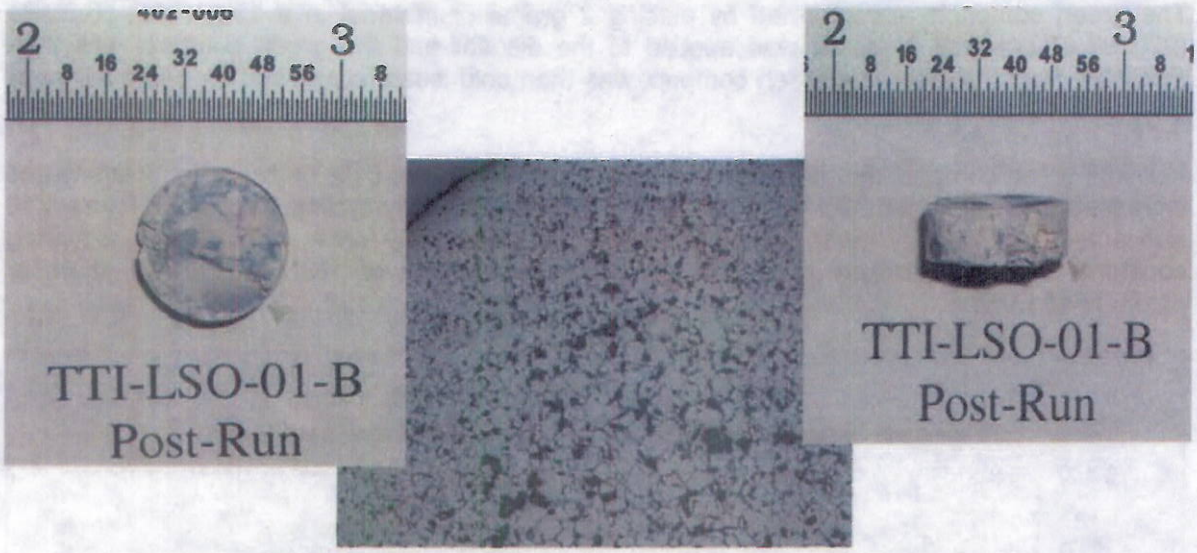

Figure 1.11. Photos showing macroscopic cracking and grain structure of TTI-LSO-01-B sintered at 1850°C for 10 hours.

Cold Isostatic Pressing and Sintering Ceramic Preform Fabrication

Five compositions were prepared and are outlined in figure 1.12. The goal was to determine the effect upon of dopant and processing techniques upon grain growth and density. Two dopants or grain growth enhancement oxides where evaluated. Calcium and magnesium oxide where prepared in 0.5% and 2% in molar ratios. Source material for calcium oxide doping was prepared by dissolving $Ca(NO_3)_2$ *H_2O in ethanol. Then LSO was added to the solution and mixed for one hour. The mixture was dried overnight on a hot plate at 250°C. Source material for magnesium oxide was prepared by the same method as above with a magnesium source of $MgCO_3Mg(OH)_2$*H_2O.

Chemical composition
Lu_2SiO_5
Lu_2SiO_5+0.5%CaO
Lu_2SiO_5+2%CaO
Lu_2SiO_5+0.5%MgO
Lu_2SiO_5+2%MgO

Figure 1.12, list of the compositions prepared for cold isostatic pressing and sintering evaluations.

The green compacts were formed by placing 2 grams of material in a 13mm die. 6.3MPa (920psi) of uni-axial pressure was applied to the die set and the green compact was then extracted from the die. The green compact was then cold isostatic pressed for two minutes at 170 MPa (25ksi).

Nominal green compact density after cold isostatic pressing was 51% of theoretical density and increased to greater than 93% for all compositions after thermally cycling. Located in figure 1.13 is the resultant density verse temperature for the isostatically pressed samples. Sintering constants included nitrogen atmosphere, thermal ramp rates of 1°C*min^{-1}, and a chamber pressure of 15mtorr.

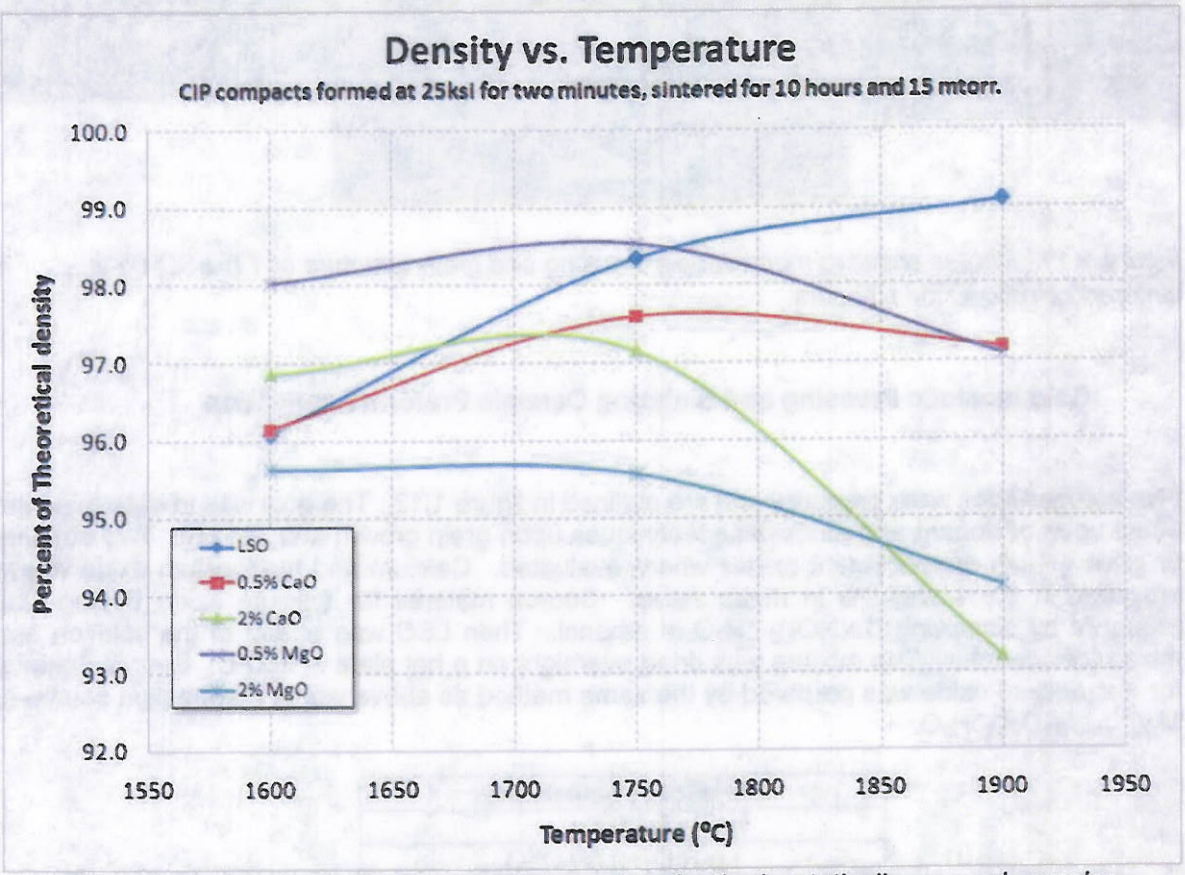

*Figure 1.13, Resultant density verse temperature for the isostatically pressed samples. Sintering constants included nitrogen atmosphere, thermal ramp rates of 1°C*min^{-1}, and a chamber pressure of 15mtorr.*

The decrease in density displayed by the doped specimens at a sintering temperature above 1750°C, can be explain eutectic melting of the dopant. Similar to other material systems that are sintered with a dopant to a liquid phase to promote densification, an optimum temperature produces the maximum densification. The decrease of density at high temperatures is a resultant of vaporization losses of the dopants.

Located in figure 1.14 and 1.15 is the resultant grain growth as a function of time to the one half. Magnesium oxide at the two percent level is contained in a separate figure due to an order of magnitude greater in grain growth. A thermal ramps of 1°C*min^{-1} was selected in attempt to minimize cracking problems that have been previously observed.

This concludes the bulk of the work in ceramic densification of the project. In summary the evaluation of temperature, composition, pressure, and time were completed for hot pressing and the effect of dopant and dopant level for cold isostatic pressing. Hot pressing yielded theoretical dense compacts, while the best achieved CIP compacts was 99%. The multiple HP conditions yielded a theoretical dense 4% cerium doped ceramic LSO perform, with temperature having the largest effect on grain growth. An increase in grain size with increasing hot press applied pressure was not predicted with the previously discussed equations and will be reevaluated through additional experiments at the conclusion of the project if time permits.

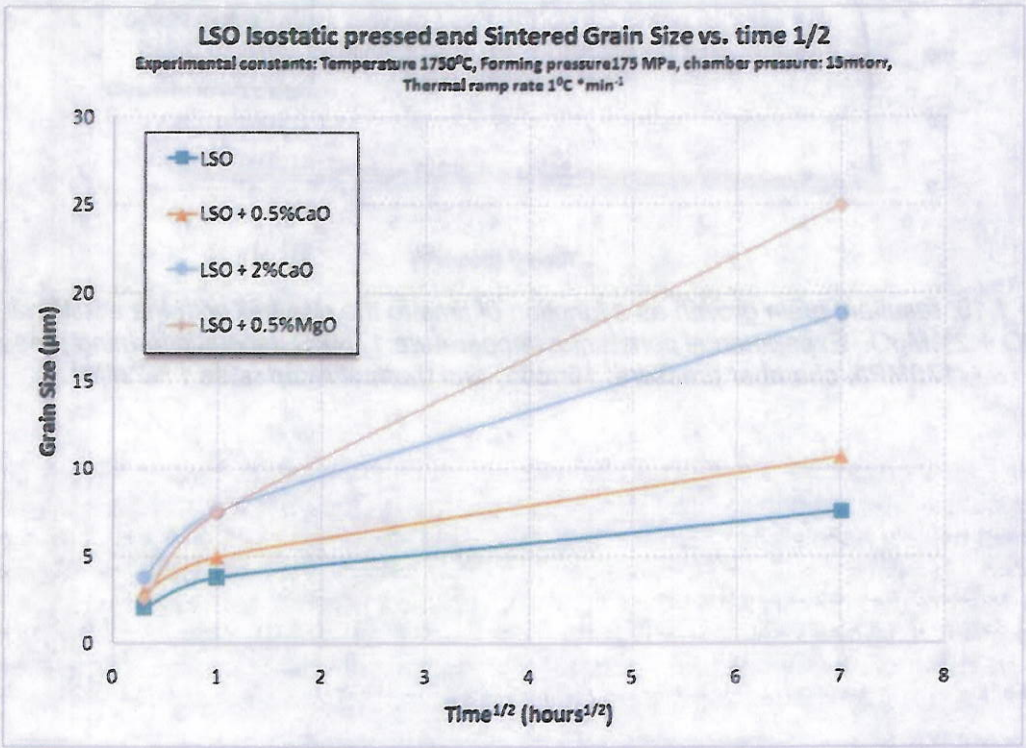

*Figure 1.14, resultant grain growth as a function of time to the one half. Experimental constants: temperature:1750°C, Isostatic forming pressure 175MPa, chamber pressure: 15mtorr, and thermal ramp rates 1 °C*min^{-1}.*

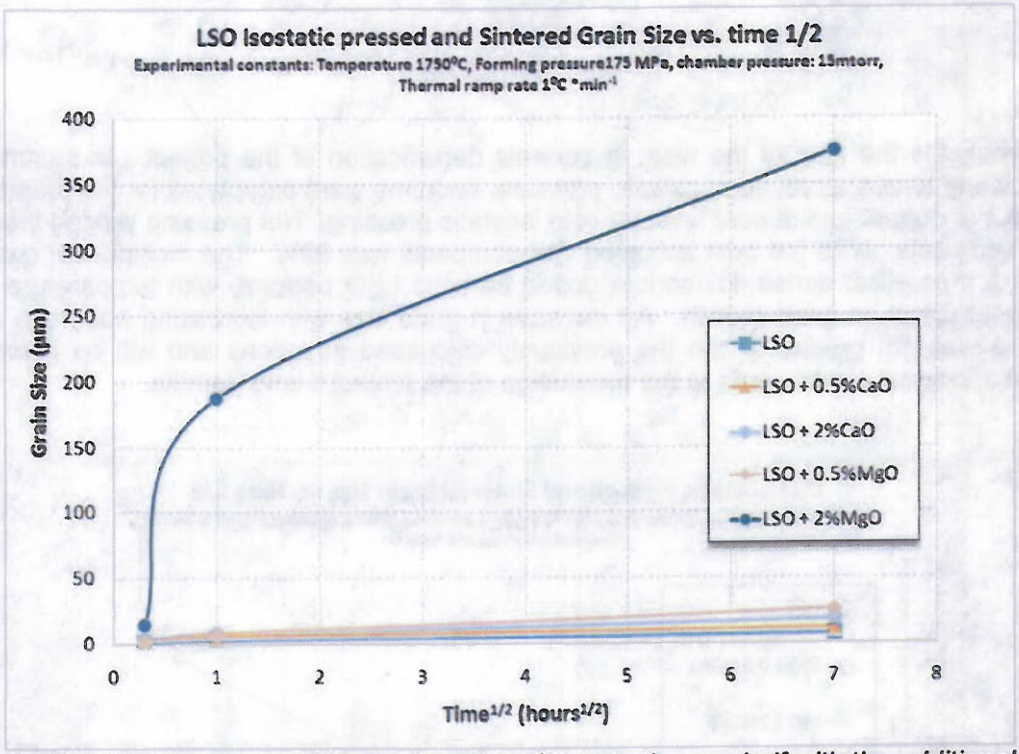

*Figure 1.15, resultant grain growth as a function of time to the one half with the additional plot of LSO + 2%MgO. Experimental constants: temperature:1750°C, Isostatic forming pressure 175MPa, chamber pressure: 15mtorr, and thermal ramp rates 1 °C*min^{-1}.*

Hot Pressing Ceramic Preform Fabrication

Three sets of HP experiments were conducted during this reporting period. Experimental constants were:

- Thermal ramp rate= 5°C/min
- Chamber pressure during pumpdown = 3-4 mTorr
- Gas ambient = nitrogen
- Die diameter: 28.6 mm (1.125 in)
- Die material: SGL-7510 Graphite
- Amount of source material:15 grams

Experimental variables for the HP study included particle size, temperature, time and applied pressure. Figure 1.16 summarized the experimental parameters, measured density and theoretical density (expressed in terms of percentage of theoretical density) for the initial set of experiments.

Figure 1.16. Initial HP Processing Study, dwell time at temperature and pressure is constant at 1 hour.

Experiment	Chemical Composition	Temperature (°C)	Force (MPa)	Density (g/cm^3) and % of theoretical density
HP131-LSO4	Lu2SiO5 (Batch A.1)	1600	10	7.359 (99.4%)
HP161-LSO5	Lu2SiO5 (Batch A.1)	1600	10	7.158 (96.7%)
HP162-LSO6	Lu2SiO5 (Batch A.1)	1500	10	6.542 (88.4%)
HP163-LSO7	Lu2SiO5 (Batch A.1)	1400	10	5.783 (78.1%)
HP164-LSO8	Lu2SiO5 (Batch A.1)	1600	20	7.554 (>100%)
HP165-LSO9	Lu2SiO5 (Batch A.1)	1700	10	7.602 (>100%)
HP166-LSO10	Lu1.99Ce.01SiO5 (Nano + 1% Cerium)	1600	10	7.208 (>100%)
HP167-LSO11	Lu1.98Ce.02SiO5 (Nano + 2% Cerium)	1600	10	7.379 (99.7%)
HP168-LSO12	Lu1.96Ce.04SiO5 (Nano + 4% Cerium)	1600	10	7.198 (97.3%)

Using the HP process the cracking problems which had been prevalent with the CPS approach were not observed. Figure 1.17 shows a typical LSO preform produced by the HP method. Figure 1.18 is a micrograph of the cross section of HP131-LSO4, formed at 1600°C, 10 MPa, for 1 hour dwell.

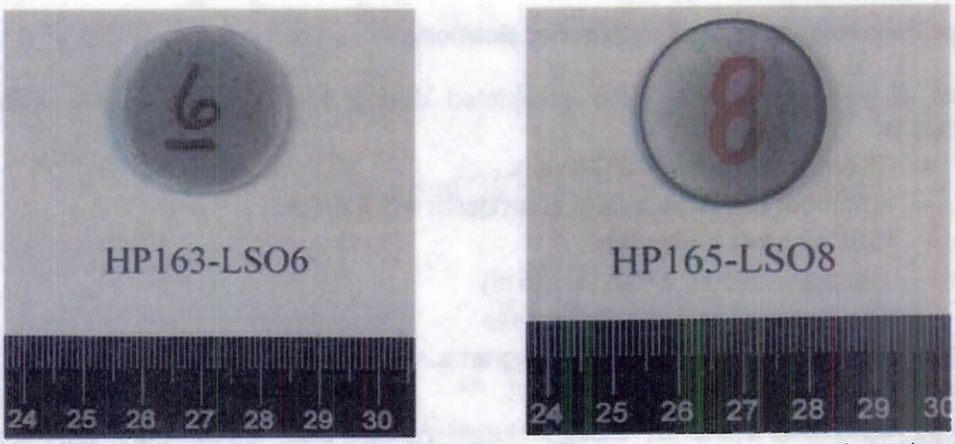

Figure 1.17. LSO samples from the initial HP study. There were no observed cracks on the surface or cross sections of the samples

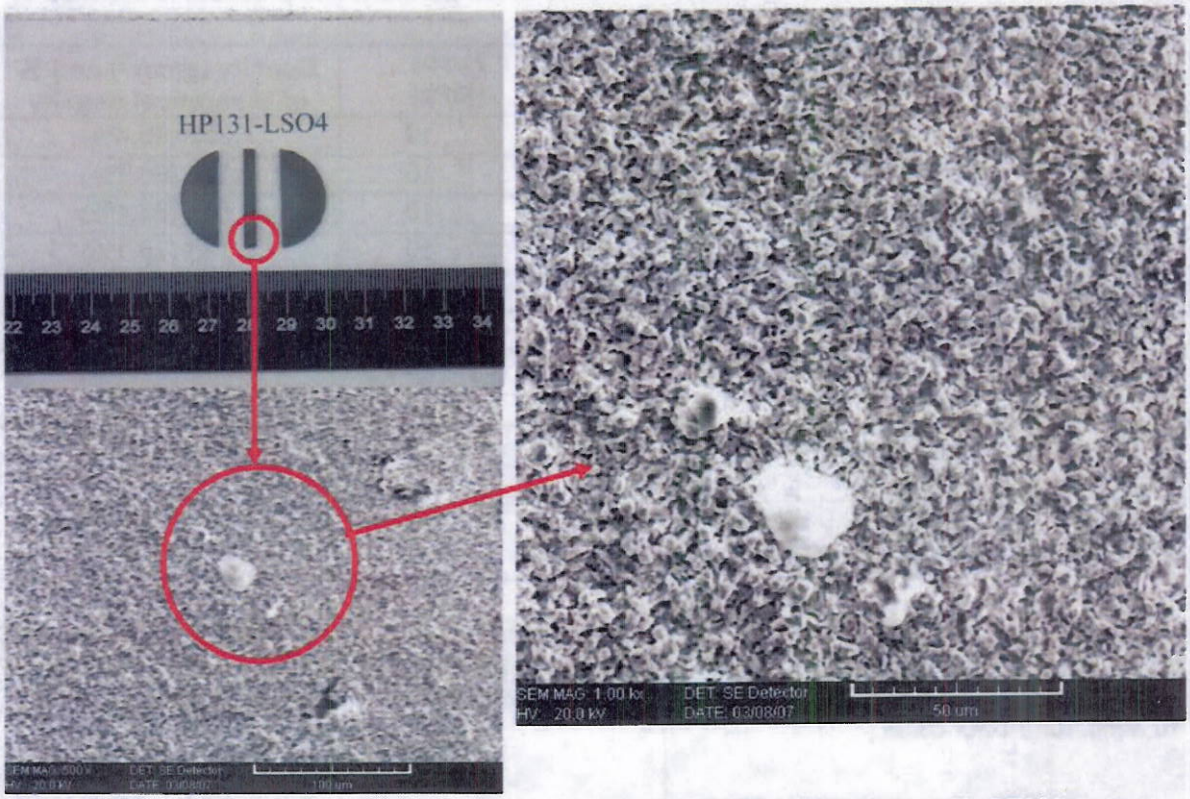

Figure 1.18. Photograph showing sections taken from HP131-LSO4 along with SEM images showing grain structure. Note that no macroscopic cracks were observed in this sample.

Initial experiments showed an increase in density with increasing temperature for undoped (i.e. no cerium added) as shown in Figure 1.19. Figure 1.20 shows the observed decrease in density with increasing cerium levels (1600°C, 10 MPa, one hour dwell).

Note that the decrease in density with increasing cerium concentration observed for hot pressing is opposite the trend observed for the CPS process.

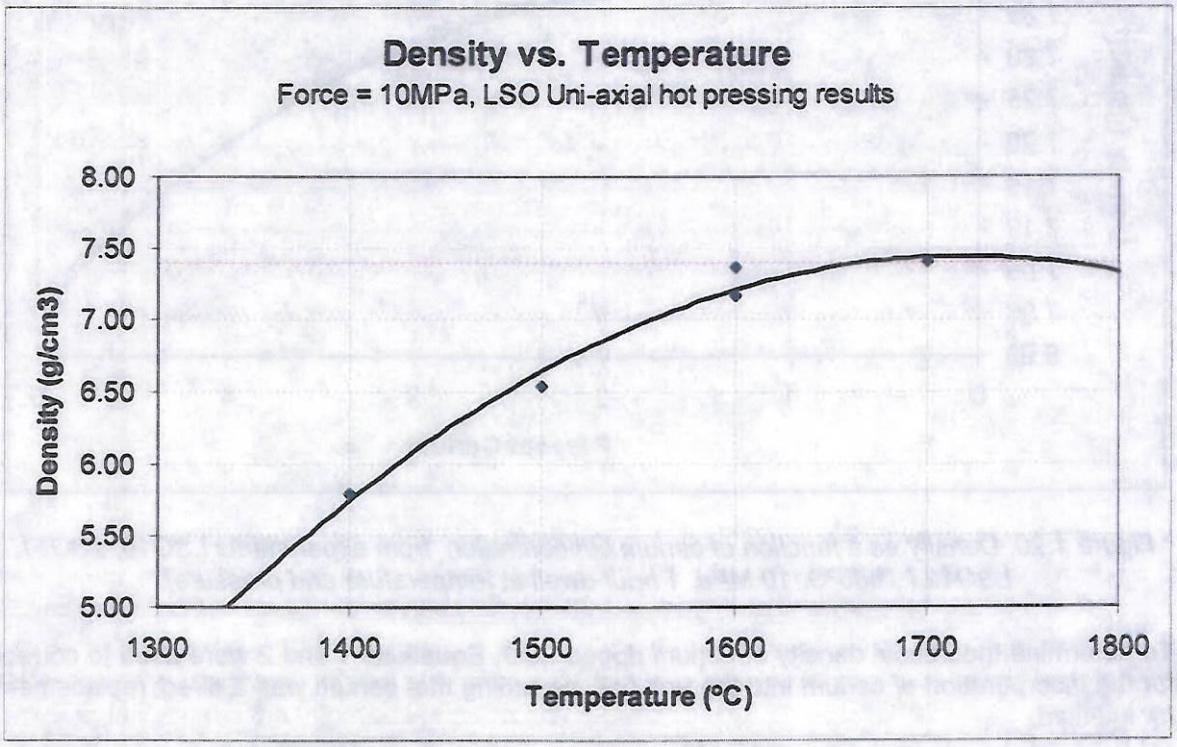

Figure 1.19. Undoped LSO, data from experiments LSO4, LSO5, LSO6, LSO7, LSO9, constants include 10MPa, 15 grams of source powder and 1 hour dwell at temperature and pressure.

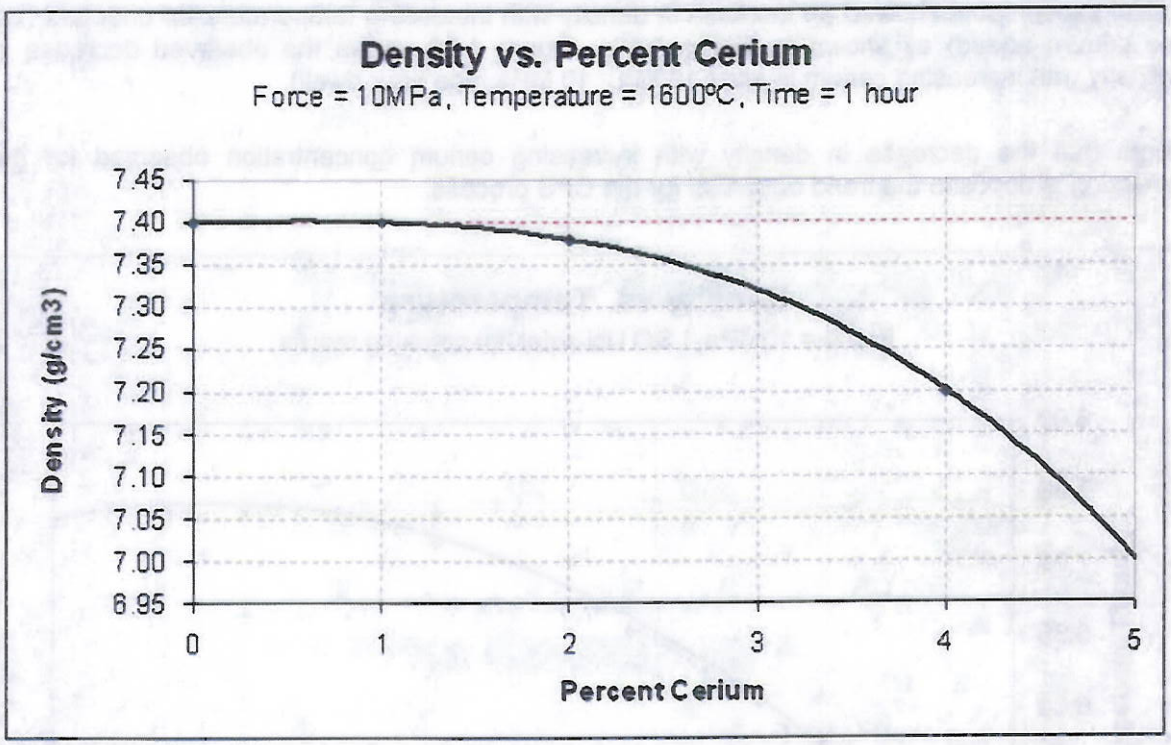

Figure 1.20. Density as a function of cerium concentration from experiments LSO10, LSO11, LSO12 (1600°C, 10 MPa, 1 hour dwell at temperature and pressure).

To determine theoretical density of cerium doped LSO, Equations 1 and 2 were used to correct for the incorporation of cerium into the unit cell, assuming that cerium was a direct replacement for lutetium.

$$\rho cal = \frac{MZ}{V} \times 1.6602 g\ cm^{-3} \qquad \text{Equation. 1}$$

Calculated cell volume:

Cubic: $V = a_0^3$

Monoclinic: $V = a_0 b_0 c_0 \sin b$

Calculated cell mass:

$M = x_a M_a + x_b M_b + x_n M_n + \ldots$

Were M_a, M_b, M_n .... are molecular weights and x_a, x_b, x_n.... which represent the fraction of a mole of each chemical component. Z is simply an interger and is used to indicate the number of atoms within a unit cell.

Once theoretical densities where obtained for both Lu_2SiO_5 and Ce_2O_3 the composite density was obtain by Equation 2.

$$\rho cal_{total} = (\rho cal_{Lu2SiO5} * 1\text{-}X) + (\rho cal_{Ce2O3} * X) \qquad \text{Equation 2}$$

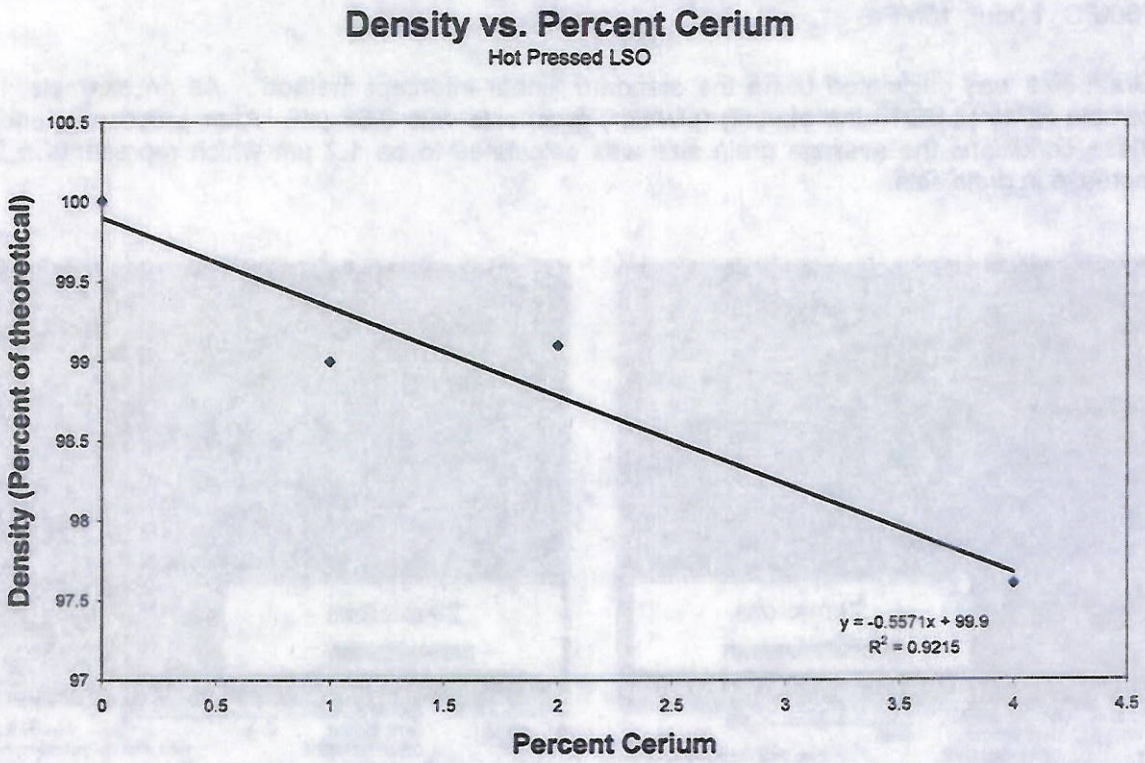

Figure 1.21., Corrected preform density using Equations 1 and 2. Data from experiments LSO10, LSO11, LSO12, constants include 1600°C, 10 MPa, 1 hour dwell at temperature and pressure 1600°C, 10MPa, 1 hour dwell time.

With an increase level of cerium the density of the preform was found to decrease as shown in Figure 1.21 and summarized in Equation 3, where ρ is the percent of theoretical density, and x is the percent of cerium.

$$\rho = -0.5571x + 99.9 \qquad \text{Equation 3}$$

Note that for the conditions used for the cerium doped preforms, undoped LSO yielded theoretical dense performs.

Based on this observation a second set of experiments were conducting in which temperature, pressure or time were increased to explore the effects of these parameters on perform density for cerium doped performs. For the second set of HP experiments, source material processing was also refined with the goal of reducing source particle size.

The microstructure of the ceramic performs was characterized using scanning electron microscopy.

Figure 1.22 contains micrographs at various magnifications of HP192-LSO15, formed at 1600°C, 1 hour, 10MPa.

Grain size was calculated using the standard "linear intercept method". As an example, for sample HP192-LSO15 the starting (powder) grain size was 0.62 μm. After processing under these conditions the average grain size was calculated to be 1.2 μm which represents a 2X increase in grain size.

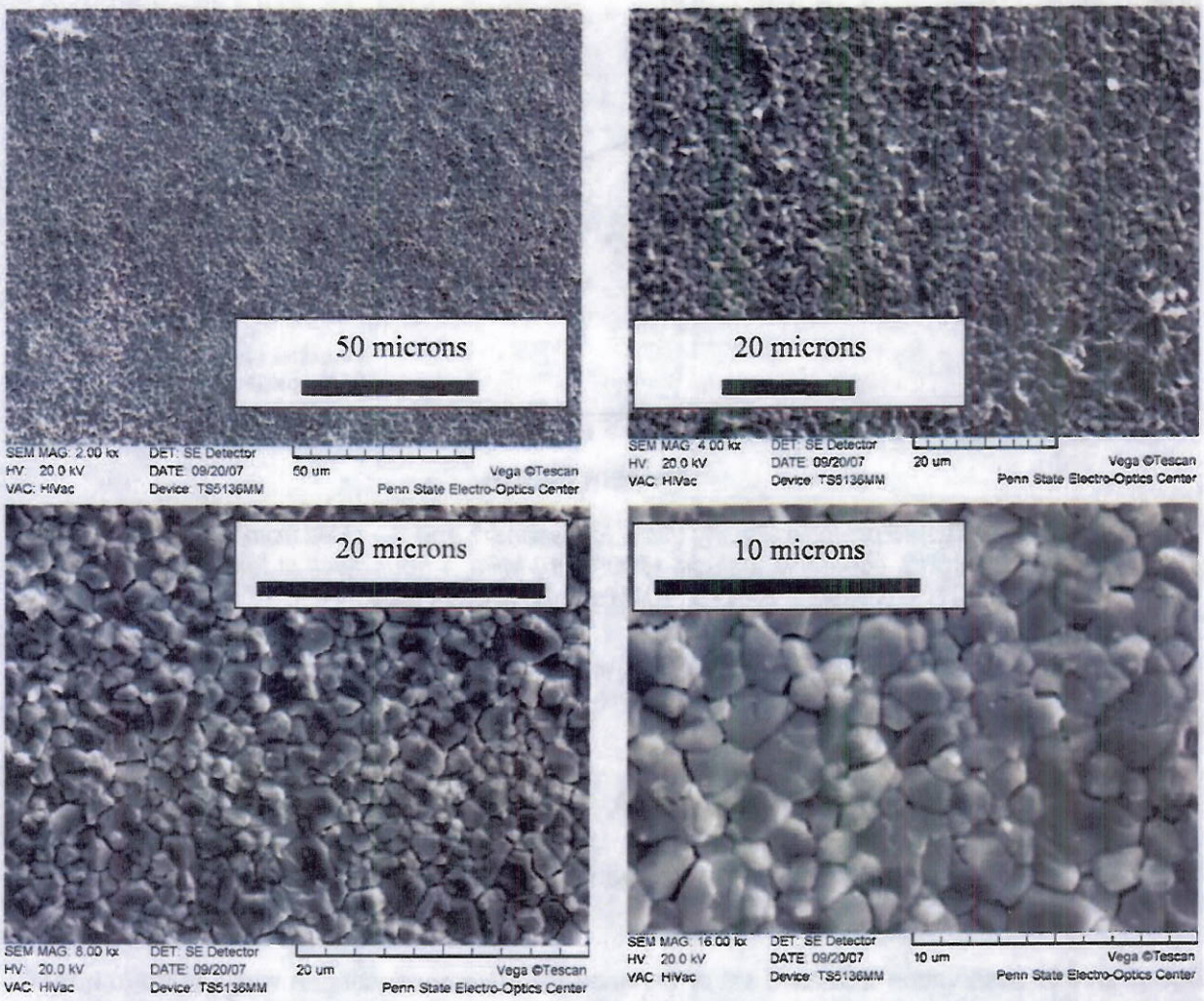

Figure 1.22. SEM micrographs of HP192-LSO15, hot pressed at 1600°C, 10 MPa, at a one hour dwell, chemical composition Lu_2SiO_5.

In summary for un-doped LSO:

- LSO preform having theoretical density were obtained by hot pressing at conditions outlined in figure 1.23.
- Hot pressing LSO has been demonstrated to be a viable method for producing a dense ceramic performs.
- Density of the preform increases with increasing temperature, time, and forming pressure.
- For the range of parameters that were studied, temperature had the largest effect on density.

Figure 1.23. Hot press parameters that produced a theoretical dense preform

Temperature	Pressure	Dwell Time
1700	10	1
1800	10	1
1600	20	1
1600	10	5.5

Seed Attachment and Growth Initiation

Seed attachment and growth initiation are key steps to promote directional SSR over large areas. Previous experience indicated that internally seeded ceramic performance often suffers from stress cracking as the result of the change in volume upon densification of the ceramic. The plan for this program was to focus the effort on externally seeding of the process by bonding a polished seed to a polished surface of the ceramic preform and holding the two materials together under a mechanical load while heating to an elevated temperature. However, due to ani-isotropic thermal expansion along the primary crystallographic orientation, it was necessary to use internally seeding.

External Seeding

Externally seeding was completed by bonding a polished seed to a polished surface of the ceramic and holding the two materials together under a mechanical load while heating to an elevated temperature.

In previous materials we have found that the surface finish, mechanical load, atmosphere and temperature-time history impact the ability of the seed and preform to effectively bond prior to the progression of SSR.

The effect of temperature, time, applied pressure, and seed composition were evaluated. Three vendors supplied single crystals (seeds) for the SSR experiments. Sinoceramic supplied Lu1.8Y0.2SiO5 (LYSO) at the below specifications.

- Size: 2 x 2 x 10 mm3
- Crystal orientation: (001) on 2 x 2 face
- Flatness: for all surfaces 5 waves PV
- Surface roughness: 20-40Å
- Scratch-dig for all surfaces: Surface quality 60-40 per MIL-PRF-13830

However the seed were not (001) orientation, located in figure 1.31 is the Wulff surface normal of the 2 x 2 mm face. If the crystal was properly oriented, the (001) would be located at point A. The (20-1) orientation is approximately 14° off the center in the x axis and 10° off the Y axis. Determining the misorientation between the as supplied and specified orientation results in an interplanar angle between (20-1) and (001) of 79°. The notations upon the SN projections are as follows, the X axis corresponds to the in plane beam pole and the Y axis is perpendicular to the beam.

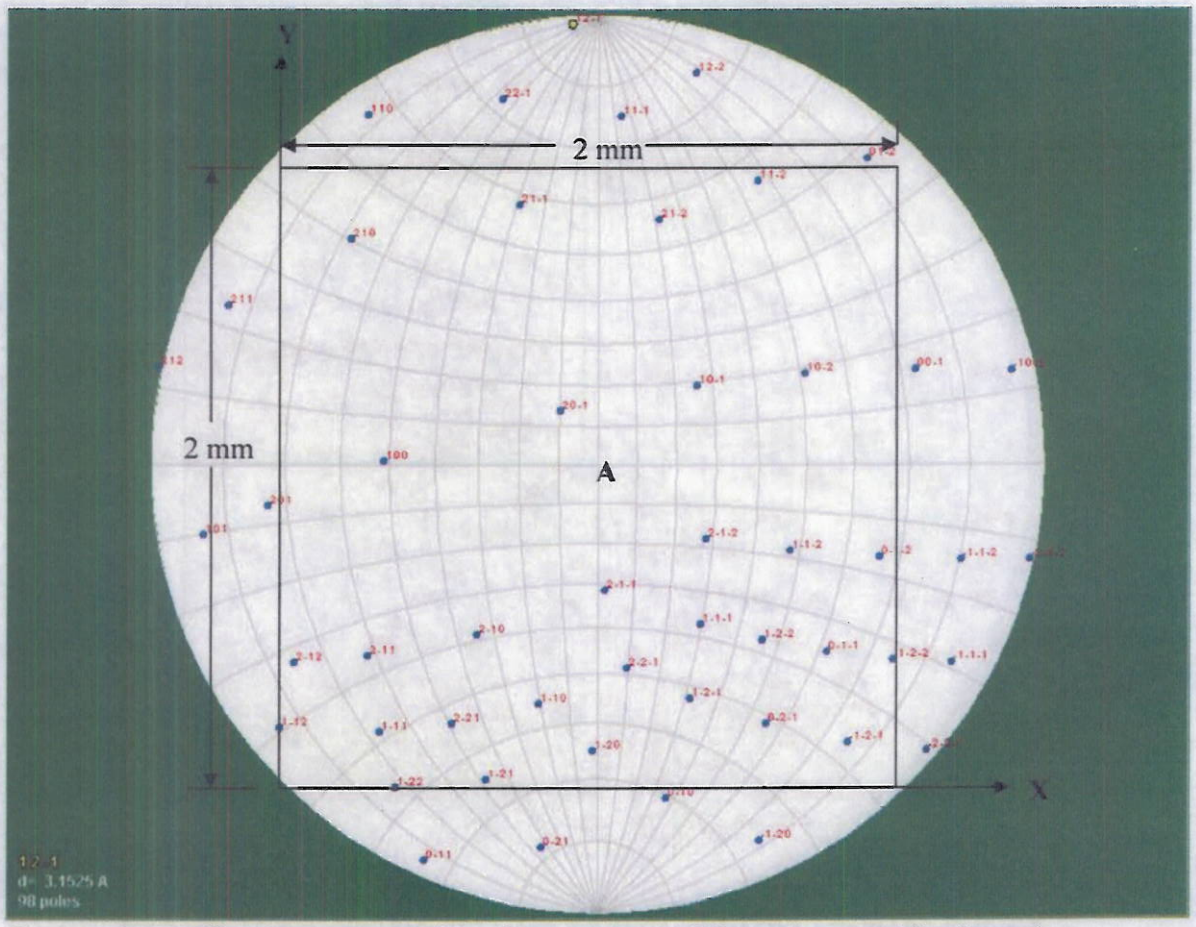

Figure 1.31 Wulff surface normal of the Sinocermics LYSO single crystal 2 x 2 mm face.

An LSO single crystal was supplied by MTI Corporation at the following specifications:

- Size: Ø25mm x 1mm thick
- Crystal orientation: (001) on Ø25mm
- Flatness: for all surfaces 5 waves PV
- Surface roughness: 20-40Å
- Scratch-dig for all surfaces: Surface quality 60-40 per MIL-PRF-13830

Similar to the LYSO seeds the orientation was not supplied as specified, rather an orientation (302) was found with the Wulff surface normal projection, see figure 1.32.

Since the first two purchased seed where not supplied at the desired orientations an additional boule segment was purchase from Siemens. While waiting for the Siemens seed crystal the MTI LSO crystal was cut into 5mm x 5mm x 1mm cubes and the LYSO seed was cut into four equal pieces.

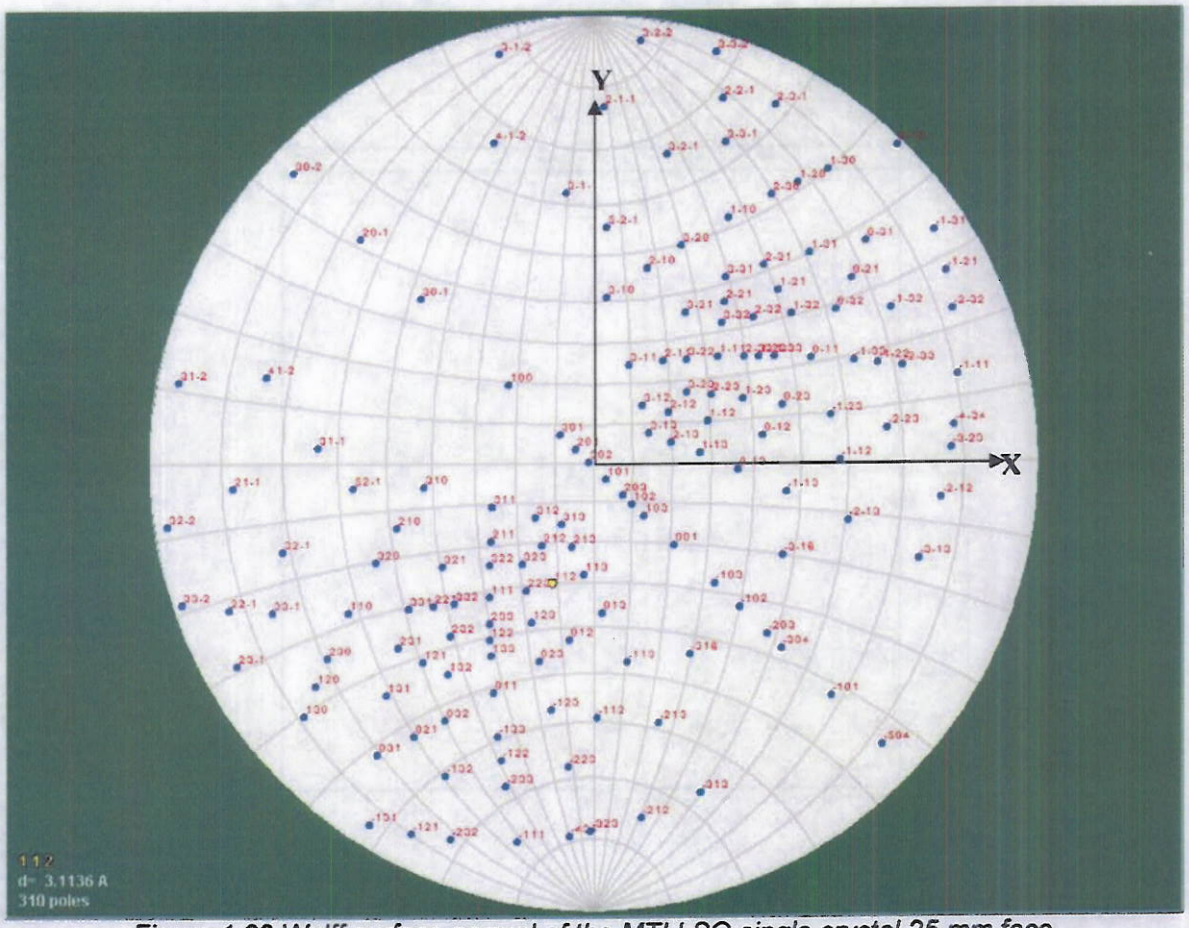

Figure 1.32 Wulff surface normal of the MTI LSO single crystal 25 mm face.

The LSO seed crystal purchase from Siemens has dimensions of 80mm diameter and 25 mm thick. This would allow for sufficient material to correct for any randomness of the crystal orientation to the three primary orientations of (001), (010) and (100). The supplied boule was ~10° off the (001), per the Wulff surface normal projection, see figure 1.33.

Due to the arbitrary orientation of the LYSO material the seeds where cut into four equal segments and labeled according to figure 1.34. As stated previously the MTI LSO crystal was cut into 5mm x 5mm squares.

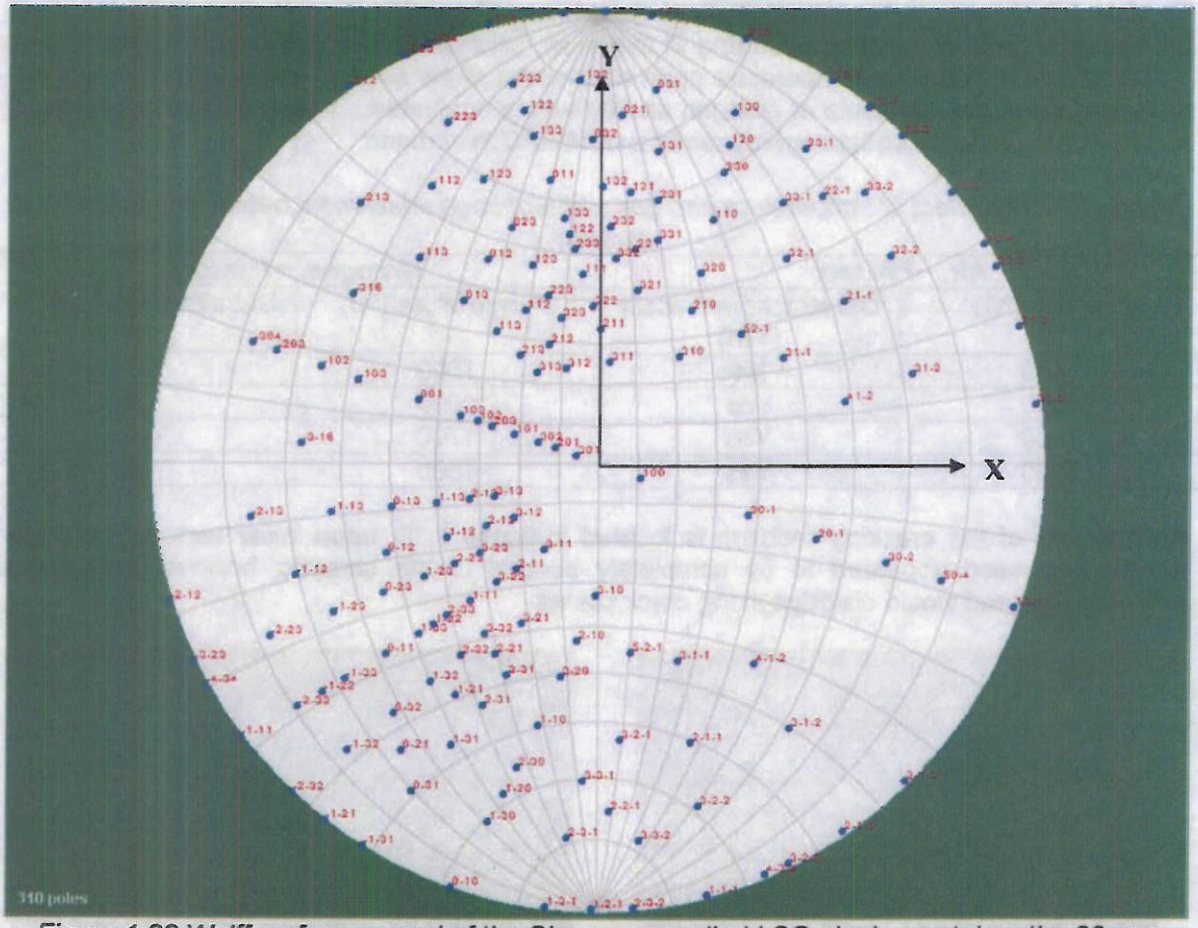

Figure 1.33 Wulff surface normal of the Siemens supplied LSO single crystal on the 80 mm face.

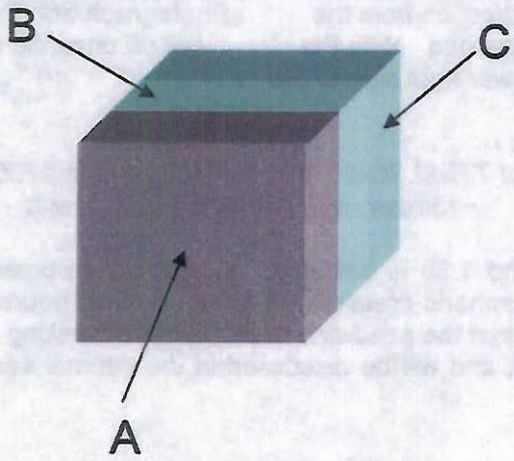

Figure 1.34, LYSO seed nomenclature used for the seed attachment experiments.

To date twenty external seed attachment experiments have been conducted, with the most problematic issue of cracking occurring in the seed, ceramic or recrystallized material. Figure 1.35 contains the effect of temperature upon attachment of the seed to the ceramic. In addition to temperature, gas ambients of nitrogen and air where evaluated. Temperatures were limited to 1700°C in air due to equipment restraints and 1800°C in nitrogen.

Figure 1.35 The effect of temperature and gas ambient upon attachment between the seed and ceramic.

Air, ~760 torr		Nitrogen, ~15mtorr	
Temperature (°C)	Did attachment occur (Y/N)	Temperature (°C)	Did attachment occur (Y/N)
1400	No	1500	No
1500	Yes	1600	No
1600	Yes	1700	Yes
1700	Yes	1800	Yes

An example of the cracking problem is located in figure 1.36, upon initial removal from the furnace the seed appeared to be completely bonded to the ceramic; however with slight pressure the seed would dislodge along crack planes.

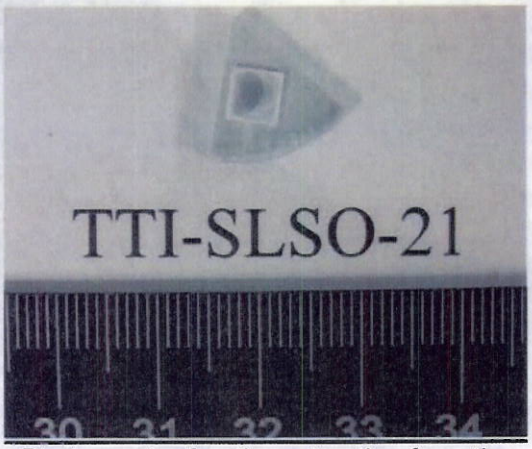

Photograph after the extraction from the furnace, with the seed attached. Note the presents of cracks in the lower right side of the seed.

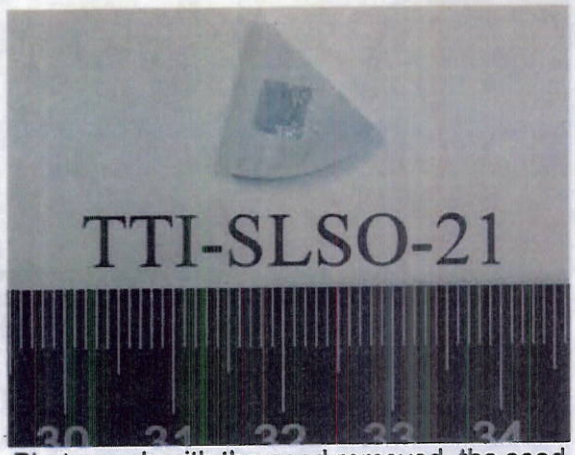

Photograph with the seed removed, the seed fell off once the composite was inverted.

Figure 1.36 Photographs of TTI-SLSO-21, forming parameters: 1700°C, 100 hours, pressure of ~15mtorr, with nitrogen gas ambient.

Located in figures 1.37 and 1.38 is the effect of attachment pressure and time, at constant temperature in air at atmospheric pressure. Less than three hours was not completed due to the cracking problem between the seed and ceramic. The cracking is related to the anisotropic thermal expansion of LSO, and will be discussed in the internal seeding section of this report. [9]

Figure 1.37 The effect of attachment pressure upon attachment between the seed and ceramic at constant temperature (1600°C) and pressure (atmospheric).	
Attachment Pressure (kPa)	Did attachment occur (Y/N)
70	No
100	Yes
140	Yes

Figure 1.38 The effect of time upon attachment between the seed and ceramic at constant temperature (1600°C) and pressure (atmospheric).	
Time (hours)	Did attachment occur (Y/N)
3	Yes
10	Yes
30	Yes
100	Yes

Internal Seeding

Experimental goals for the internal seeded SSR were to evaluated and determine, the fast crystallographical growth direction, the effect of magnesium and calcium oxide upon matrix grain size and SSR growth rate, and the effect of temperature in nitrogen gas ambient at 15mtorr.

Two molar ratios of the doped compositions where prepared at 0.5% and 2%, respectively. Source material for calcium oxide doping was prepared by dissolving $Ca(NO_3)_2 * H_2O$ in ethanol. Then LSO was added to the solution and mixed for one hour. The mixture was dried overnight on a hot plate at 250°C. Source material for magnesium oxide was prepared by the same method as above with a magnesium source of $MgCO_3Mg(OH)_2 * H_2O$.

The green compact were formed by placing 1.4 grams of material in a 13mm die and lightly pressed to create a level plane to place the seed crystal. The seed was then placed in the center of the diameter and then an additional 1.4 gram of material was placed into the die. 6.3MPa (920psi) of uni-axial pressure was applied to the die set and the green compact was then extracted from the die. The green compact was then cold isostatic pressed for two minutes at 170 MPa (25ksi).

Nominal green compact density after cold isostatic pressing was 51% of theoretical density and increased to greater than 93% for all compositions after thermally cycling.

Located in figure 1.39 is the compression of the matrix grain and recrystallization rate verse time^{½}. While the difference between the two was approximately double, the effect of dopants significantly increased the difference by an order of magnitude with the addition of both dopants at the 2% molar level, as displayed in figure 1.40.

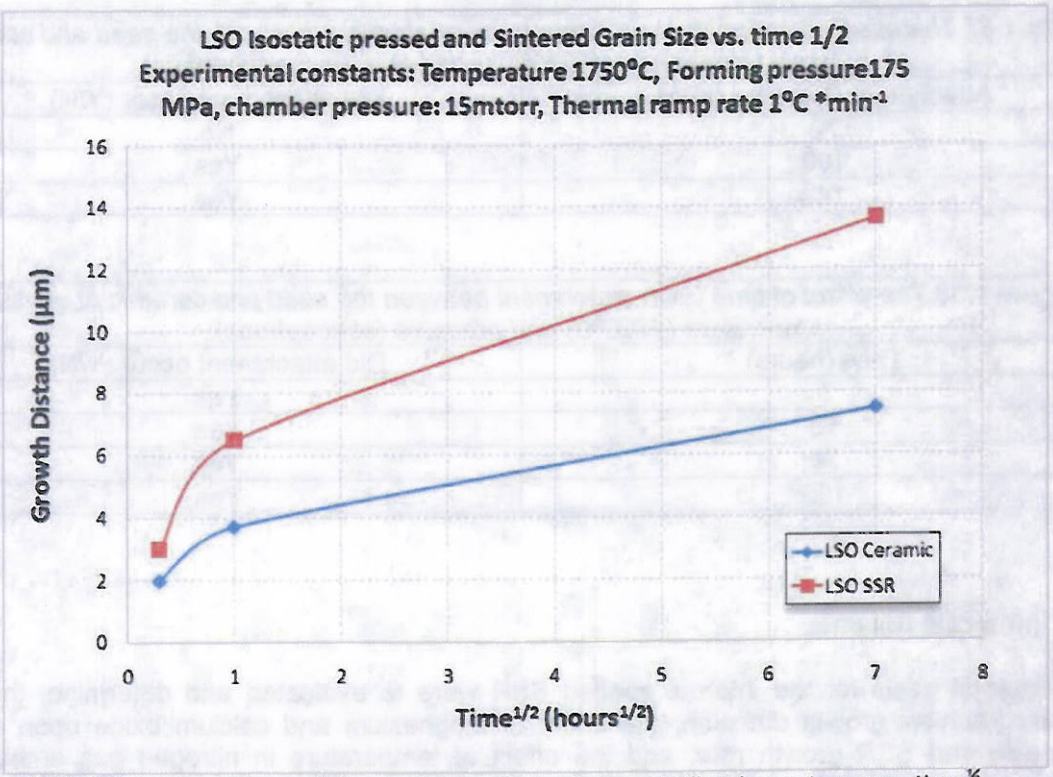

Figure 1.39. The comparison of the matrix grain and recrystallization rate verse time½

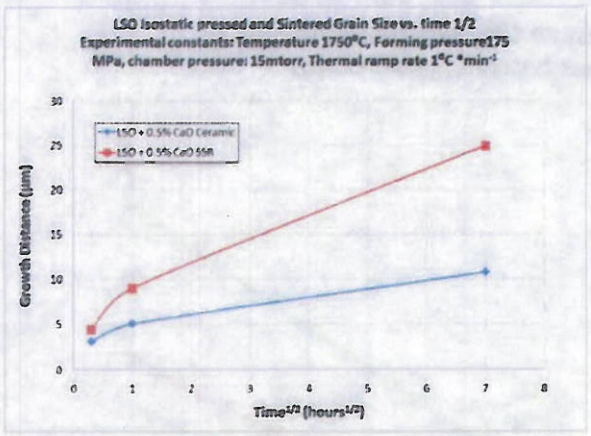

LSO + 0.5% Calcium oxide

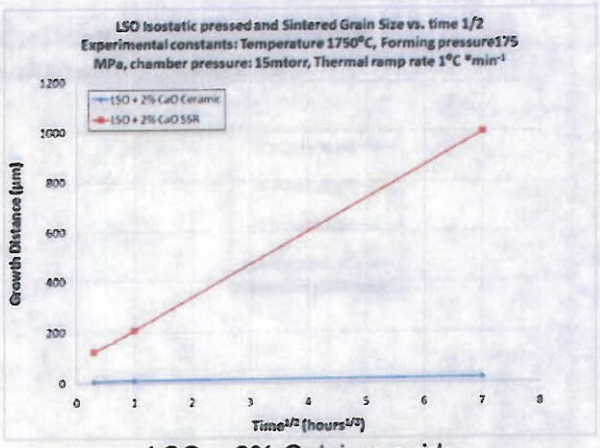

LSO + 2% Calcium oxide

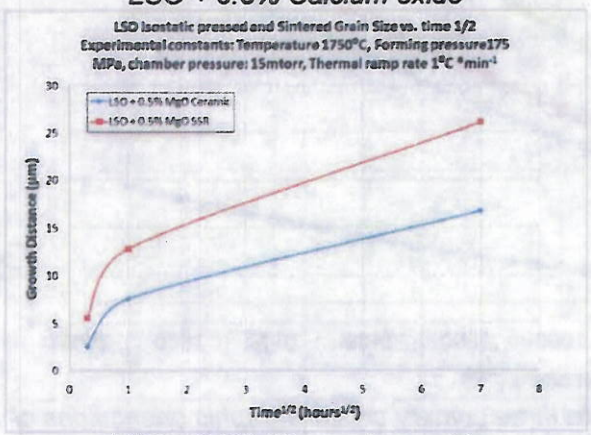

LSO + 0.5% Magnesium oxide

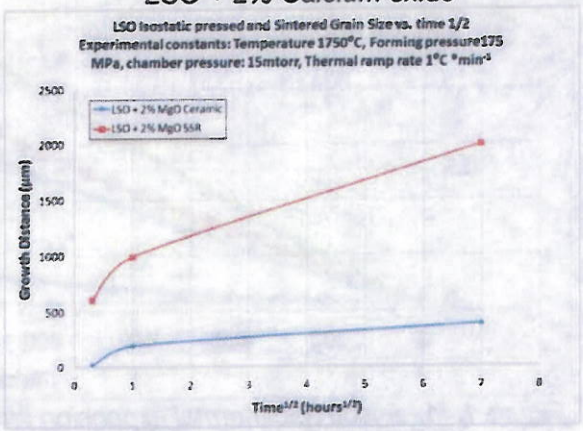

LSO + 2% Magnesium oxide

Figure 1.40, The comparison of the matrix grain and recrystallization rate verse time^{½} for dopant levels of 0.5 and 2 molar percent of calcium and magnesium oxide

The effect of dopants at the 2% level is profound, greatly increasing recrystallization rates to an acceptable level. One remaining obstacle in the growth process remains the crack formation of the recrystallized material during cooling from growth temperatures. During a systematic investigation to determining the cause of the cracks, the seed was evaluated by micrographs after each successive step during forming operations. Micrographs where taken of the seed after cutting, polishing, cold pressing, and cold isostatic pressing. No cracks or defects where found on the seed crystals.

To rule out thermal ramps rates from inducing cracks, two experiments were conducted at 1 and 5°C*min^{-1}. The seeds where unconstrained during the thermal cycles, or not embedded or attached to a ceramic compact. The relevance of unconstraint seeds is summarized in figure 1.41, in which the three primary crystallographic orientations display anisotropic thermal expansion and the ceramic was assumed to have the average. In conclusion the seed was not cracked at either thermal ramp rate, leaving the remaining variable of the stress build up between the single crystal and ceramic compact.

unconstrained

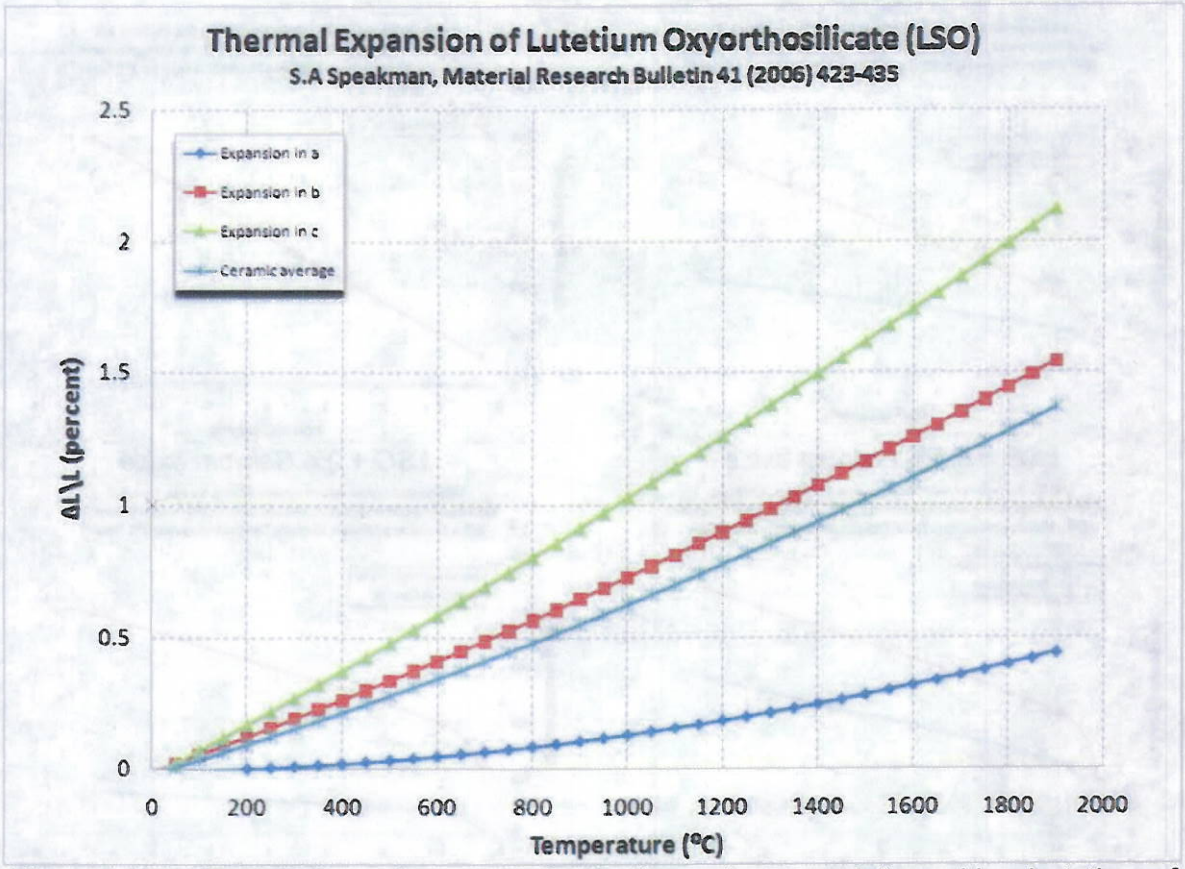

Figure 1.41, anisotropic thermal expansion for the three primary crystallographic orientations of LSO and assumed ceramic average.

Task 1 summary: Ceramic Preform Fabrication and Seed Attachment:

- Able to produce a dense LSO ceramic compact, with a cerium level up to 4 molar percent
- Increasing cerium has an inverse effect on ceramic density. Requiring either an increase in temperature by 100C or increase in pressure by 10MPa over pure LSO.
- External seeding was difficult due to thermally induced cracks.
- LSO and Ce:LSO have similar growth rates of ~4μm/hr
- Co-doping with MgO and CaO improves the growth rate to 500μm/hr and 250μm/hr

Task 2. Ce:LSO Grain Growth Kinetics

A range of parameters are known to affect the grain growth kinetics. Key parameters include growth temperature, growth direction (crystallographic orientation), dopants to enhance grain growth, processing atmosphere, and matrix grain size (surface area) influence on thermodynamic driving force. A high processing temperature will increase the grain boundary migration rate for both the primary grain and the matrix grains. If the temperature is too high the ceramic matrix grains can rapidly enlarge thus reducing the driving force. This phenomena is known as "anomalous grain growth".

The average grain size for both the matrix and for the grown crystal will be correlated to a parabolic kinetic rate equation, equation 4. The data collected for full kinetic model for grain growth has been completed based on experimental data from the internal seeded experiments. The grain growth kinetics were modeled to calculate the average grain size for the matrix and growth distance for the grown crystal using a parabolic kinetic rate equation.

$$G^2 - G_0{}^2 = (k_0 \exp(-Ea/RT))\, t \qquad \textbf{Eq. 4}$$

Where:

G	= final grain size
G_0	= initial grain size
k_0	= kinetic constant
Ea	= activation energy
T	= Temperature

The parabolic kinetic rate equation can be thought of two equations (equations 5 and 6). Which accounts for the independent effects of time and temperature.

$$G^2 - G_0{}^2 = k\, t \qquad \textbf{Eq. 5}$$

Where:

G	= final grain size
G_0	= initial grain size
k	= temperature dependant constant
t	= time

The temperature dependant constant k was described using an exponential function, Equation 6.

$$k = k_0 \exp(-Q/RT) \qquad \textbf{Eq. 6}$$

Where:

k_0	= pre-exponential constant
Q	= activation energy for boundary mobility
T	= absolute temperature
R	= gas constant

Experimental parameters for the kinetic matrix included, dopant, dopant level, time and temperature. The main objective in the SSR experiments was to create the largest difference in driving force (Δ), between the matrix grain and recrystallized crystal. This mechanism can be visualized as a two dimension example is shown in Figure 2.1. A grain with fewer than six sides will have convex boundaries and will shrink or be consumed by a larger neighbor. Where a grain with more than six sides, has concave boundaries and grow.[5].

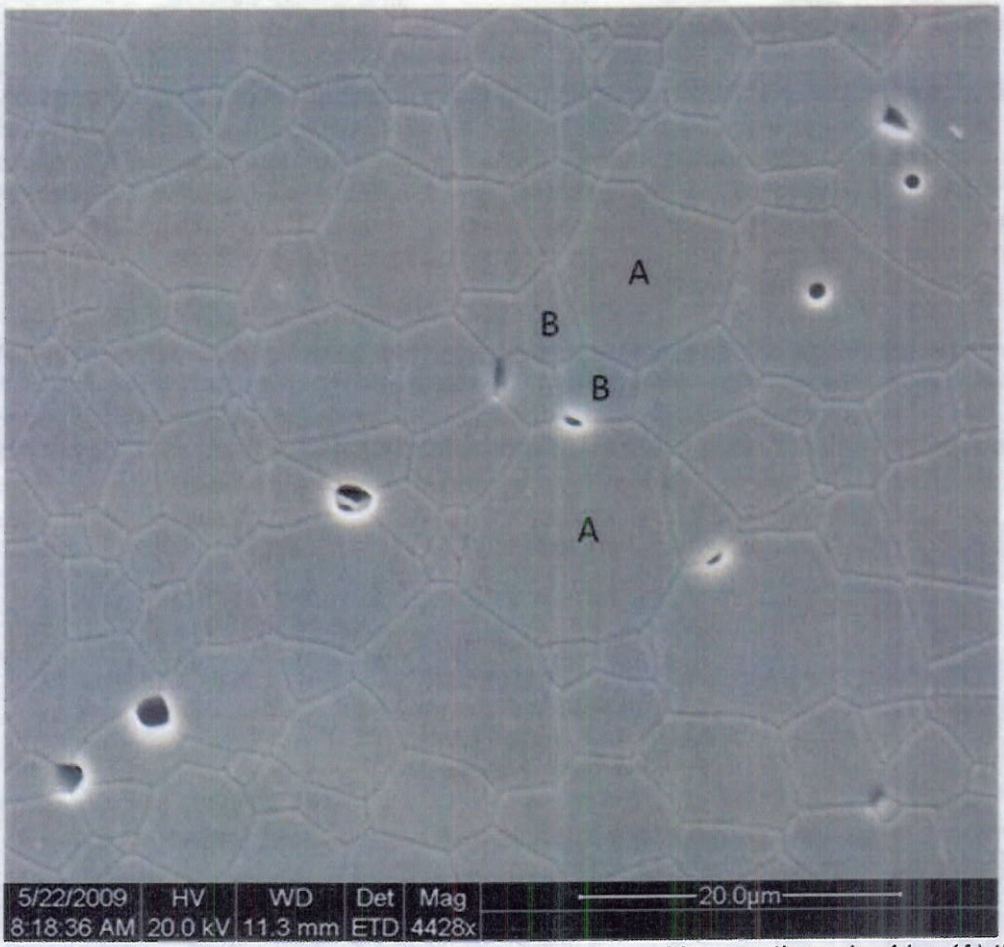

Figure 2.1 , A representative micrograph, displaying grains with more than six sides (A) that are consuming grains with less than six sides (B). The grains with six sides are currently thermodynamically stable.

For the SSR process it is imperative that the SSR area has more than six sides and the matrix grains have less than six, or the conversion to single crystal growth will not occur.

Figures 2.2 through 2.6 display the experimental results of the dopant, dopant concentration, and temperature study. Pure LSO had a Δ of 1.94, indicating that the matrix grains are impeding SSR growth and either greater temperatures or an additive is necessary to decrease the activation energy for grain boundary mobility. Compositional additives where selected to decrease the activation energy, since higher temperatures would increase the potential for exaggerated grain growth.

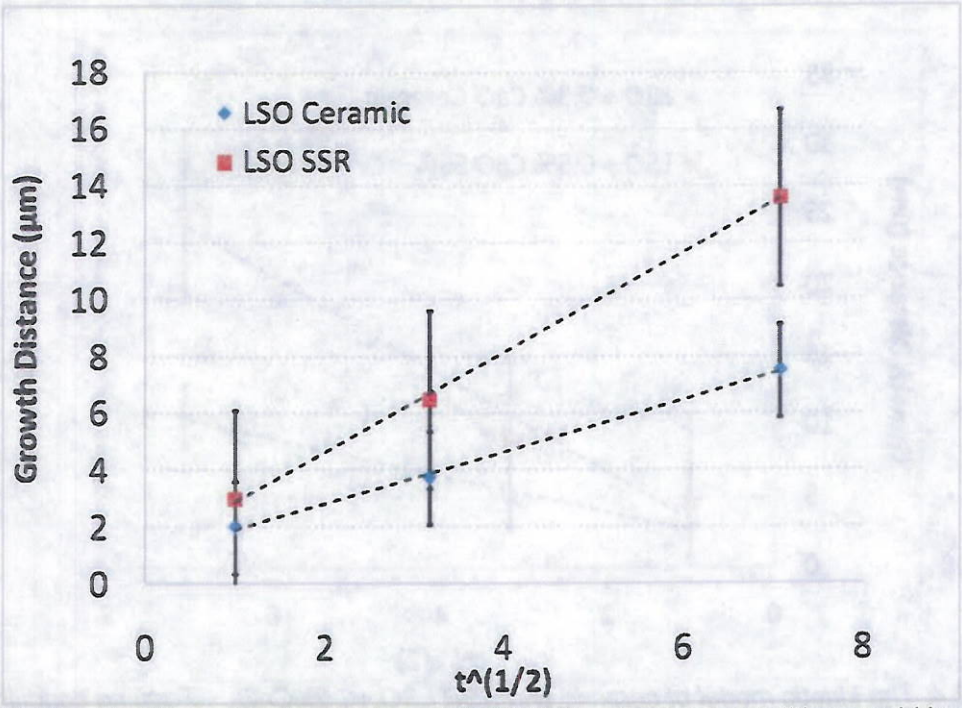

Figure 2.2, The kinetic model of ceramic and SSR LSO. Forming conditions: cold isostatically pressed and vacuum sintered at 1750°C

With the addition of MgO at 0.5%, the Δ decreased to 1.44, however; the SSR growth distance almost doubled from 14 µm for LSO to 25µm. The growth distance also doubled with CaO at 0.5% level, but the Δ increased by 29% to 2.72.

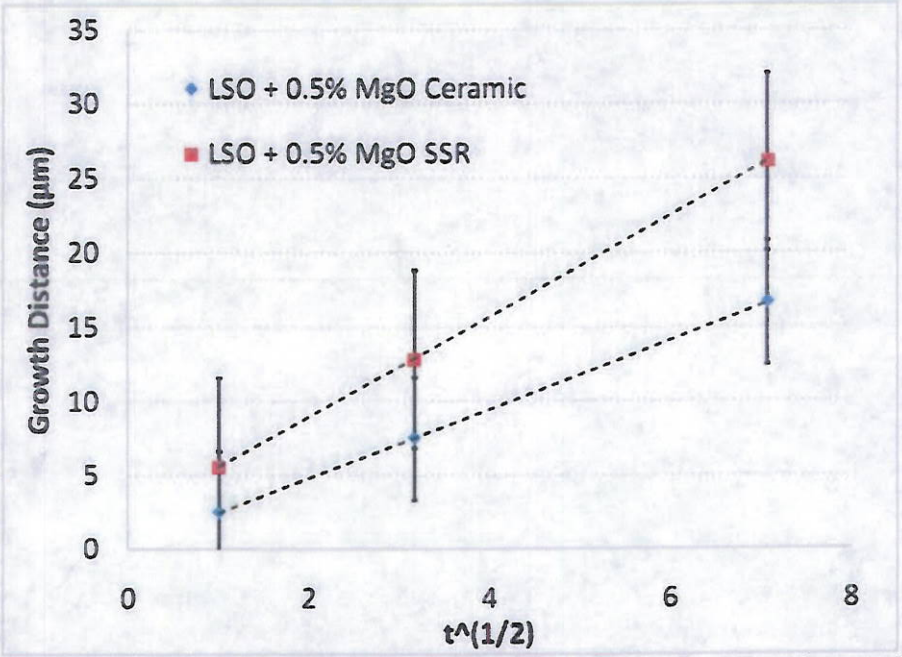

Figure 2.3, The kinetic model of ceramic and SSR LSO +0.5%MgO. Forming conditions: cold isostatically pressed and vacuum sintered at 1750°C

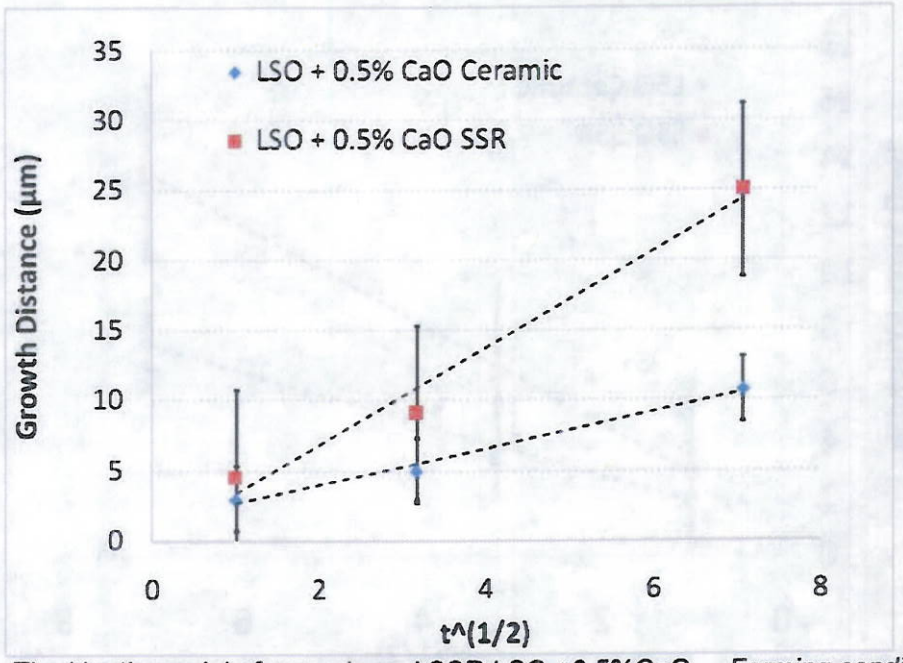

Figure 2.4, The kinetic model of ceramic and SSR LSO +0.5%CaO. Forming conditions: cold isostatically pressed and vacuum sintered at 1750°C

The dopants at the 2% level had profound effects on SSR distances. MgO had grown to 2mm at 1750°C for 50 hours, while CaO had grown to 1 mm. The significant point was with the Δ. While MgO had the largest growth distance and growth rate, the matrix grain increased to 375µm or 625x the starting particle size. The Δ increased to 3.9 for MgO at 2%. Using the simple two dimensional six sided model, SSR growth would be stopped or hindered with the large matrix grain size.

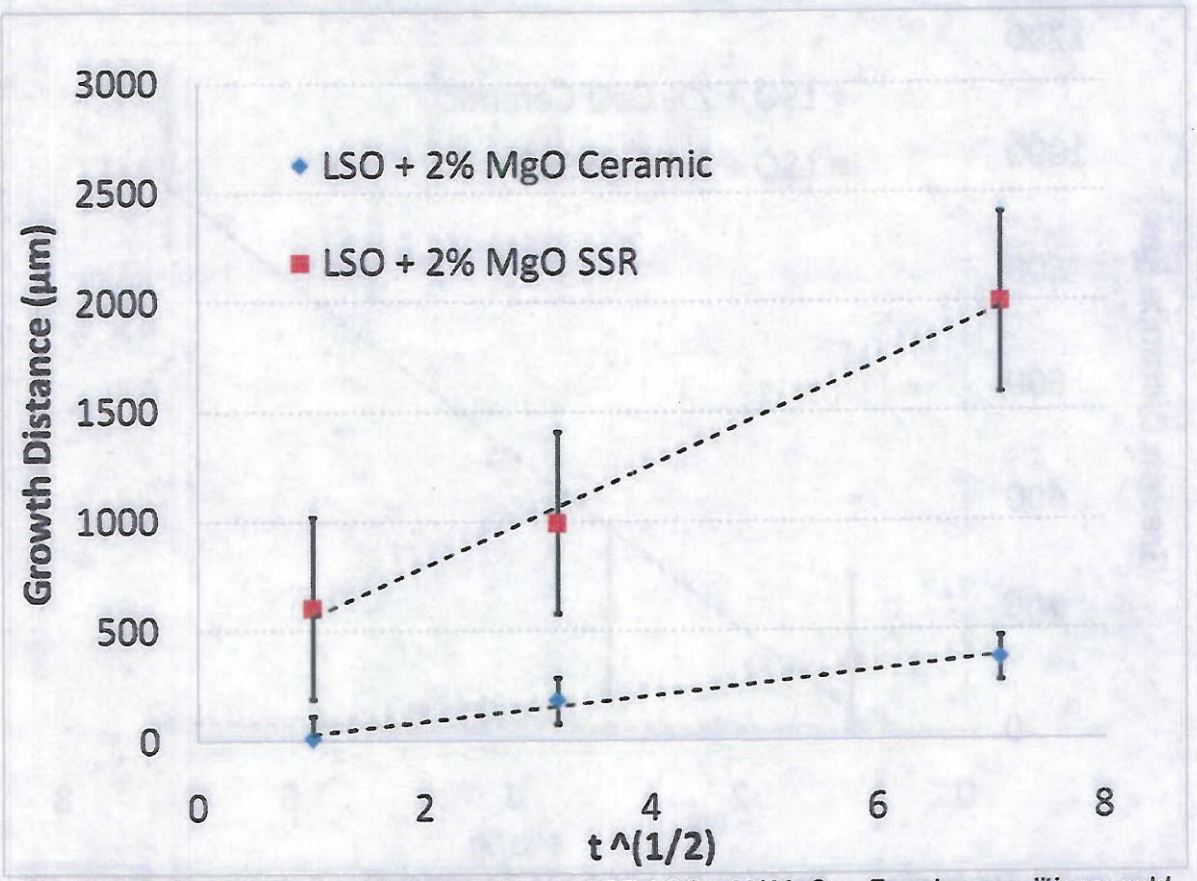

Figure 2.5, The kinetic model of ceramic and SSR LSO +2%MgO. Forming conditions: cold isostatically pressed and vacuum sintered at 1750°C

CaO on the other hand, had half the growth rate of MgO, but the Δ increased to almost 60. The increase of Δ at the 2%CaO over pure LSO was 30x. The Δ is indicating a large area LSO crystal can be produced by the SSR method, with the addition of 2%CaO. For a comparison with the previously mention MgO matrix grain size the 2%CaO grain size was 19µm.

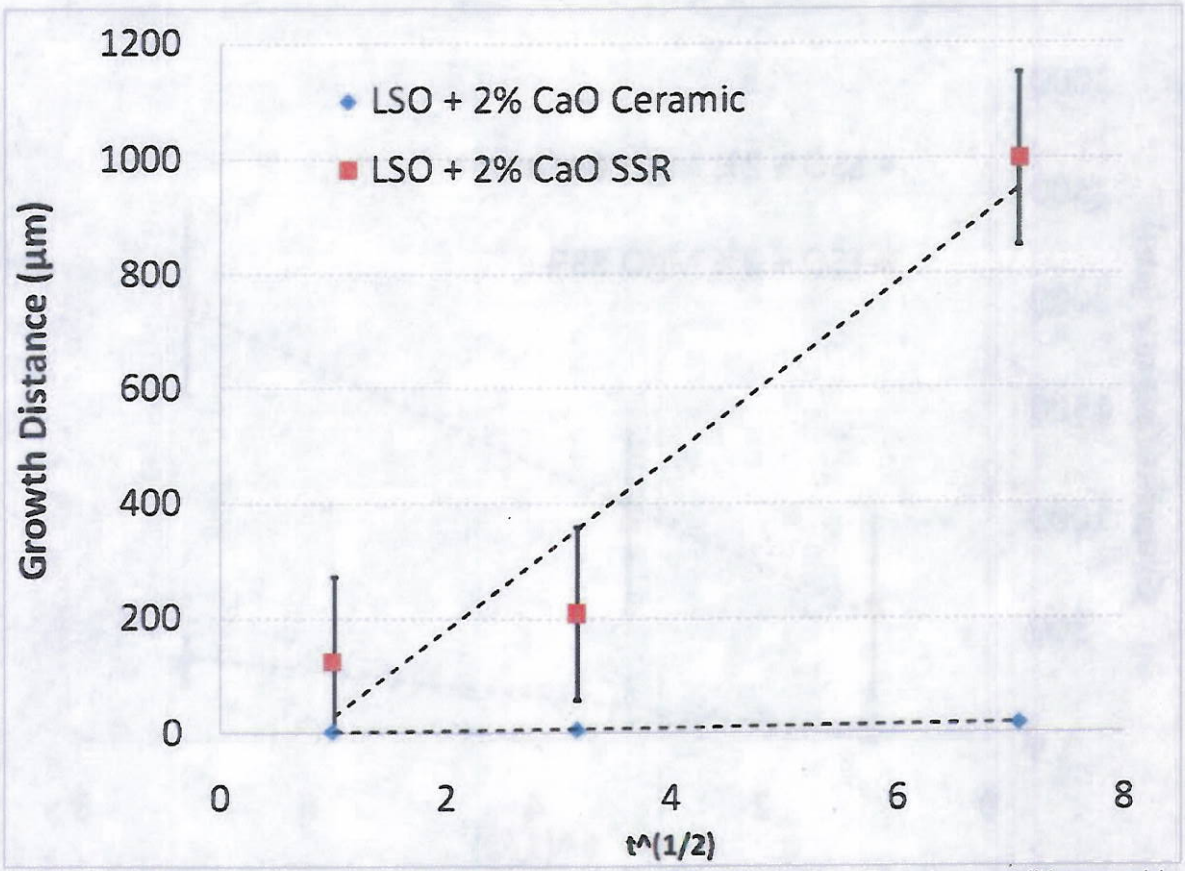

Figure 2.6, The kinetic model of ceramic and SSR LSO +2%CaO. Forming conditions: cold isostatically pressed and vacuum sintered at 1750°C

Through the use equation 6 the effect of temperature on the activation energy boundary for LSO, CaO and MgO doped LSO was obtained. The dopants reduced the energy boundary layer on average by 21%. CaO reduced the energy boundary by 24%, while MgO created an 18% reduction. Located in figure 2.7 and 2.8 is the Arrhenius plots of CaO and MgO with respect to pure LSO.

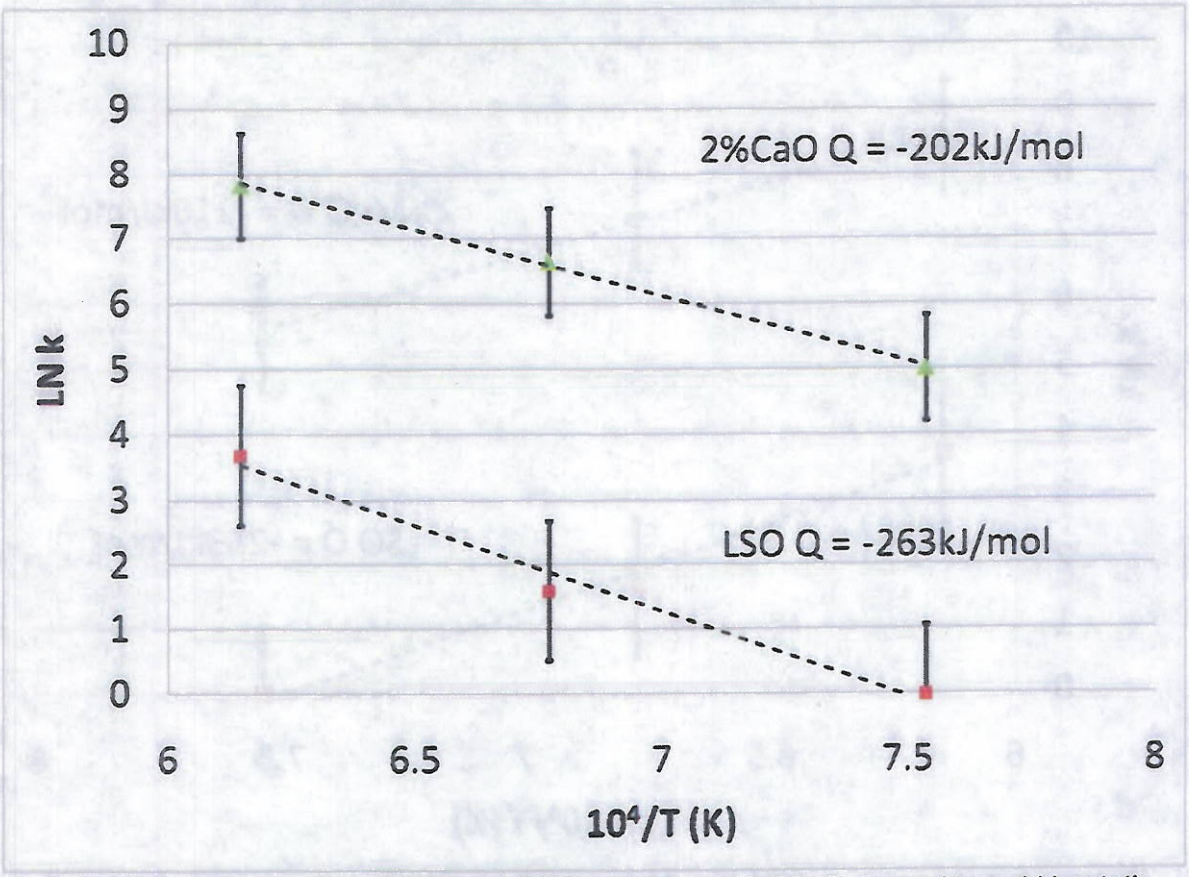

Figure 2.7, Arrhenius plot of $k=k_o exp(-Q/RT)$ of LSO and 2%CaO, formed by cold isostatic pressing and vacuum sintering for one hour.

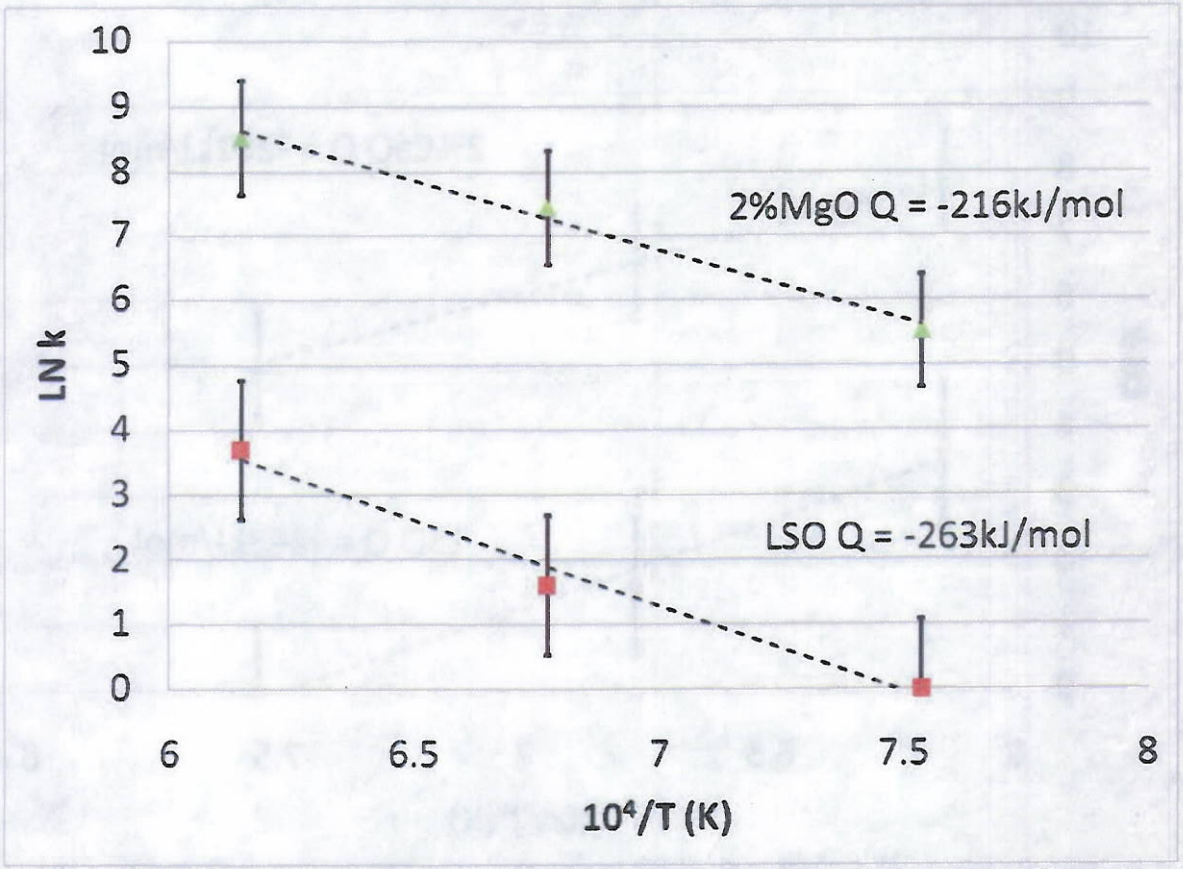

Figure 2.8, Arrhenius plot of $k=k_o exp(-Q/RT)$ of LSO and 2%MgO, formed by cold isostatic pressing and vacuum sintering for one hour.

The reduction allowed recrystallization to take place at a lower temperature than possible in pure LSO. As a comparison the activation energy for boundary mobility of LSO during hot pressing was 42kJ/mol and 4%Ce:LSO 48kJ/mol.

Using the experimentally determined rate constant and activation energy a matrix and SSR kinetic rate model was developed for all compositions. Located in figure 2.9 is the resultant equation for each composition.

Composition	Ceramic	SSR
LSO	$\Delta G = \sqrt{t(2x10^{-19}e^{0.0146T})}$	$\Delta G = \sqrt{t(6x10^{-19}e^{0.0146T})}$
LSO + 0.5%MgO	$\Delta G = \sqrt{t(2x10^{-15}e^{0.012T})}$	$\Delta G = \sqrt{t(5x10^{-15}e^{0.012T})}$
LSO + 0.5%CaO	$\Delta G = \sqrt{t(9x10^{-15}e^{0.0112T})}$	$\Delta G = \sqrt{t(5x10^{-14}e^{0.0112T})}$
LSO + 2% MgO	$\Delta G = \sqrt{t(1x10^{-12}e^{0.012T})}$	$\Delta G = \sqrt{t(3x10^{-11}e^{0.012T})}$
LSO + 2% CaO	$\Delta G = \sqrt{t(3x10^{-14}e^{0.0112T})}$	$\Delta G = \sqrt{t(9x10^{-11}e^{0.0112T})}$

Figure 2.9, the parabolic kinetic rate equation for both the ceramic grains and recrystallized material.

The kinetic model is a good fit for the experimental data, an example of the fit is located in figure 2.10 for the ceramic and SSR of LSO +2%CaO.

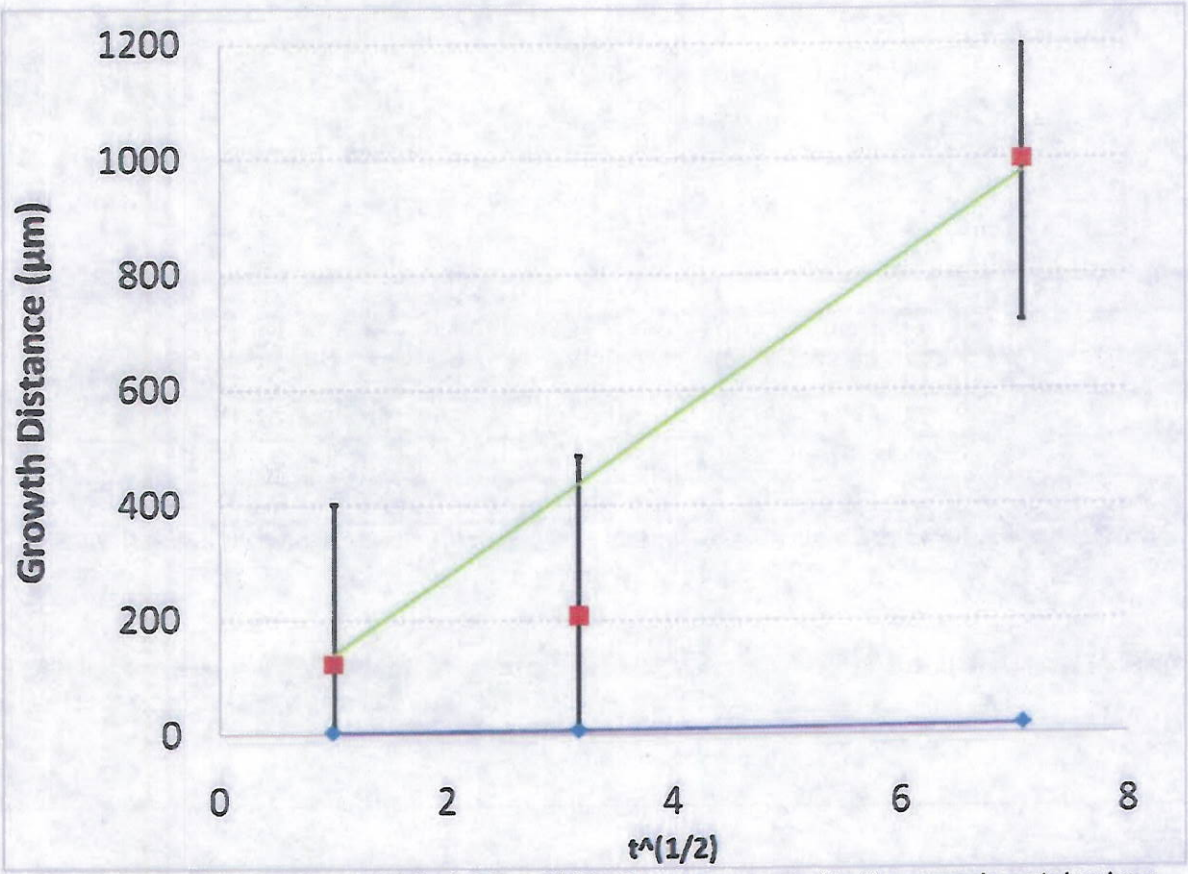

Figure 2.10, The kinetic model for LSO + 2%CaO, corresponded to the experimental values. The green curve is the SSR model and the purple is the ceramic model.

In summary for Task 2 Ce:LSO Grain Growth Kinetics:

- Dopants are the key in SSR of LSO
- Dopants at the 2% level increased the growth rate by 125x and 62.5x with MgO and CaO respectively.
- CaO is the preferred dopant, due to the greatest Δ (60X) between the SSR and ceramic.
- Dopants reduced grain boundary activation energies by ~20%.
- A predictive crystal growth model was developed for the SSR and ceramic material.

Task 3. Cerium Doping Study

Increasing cerium concentration in LSO single crystal is expected to greatly improve scintillation properties. The cerium concentration in Czochralski crystal growth of LSO is limited to <1%. Concentrations 2X-4X higher are expected via the solid state recrystallization approach resulting in significantly improved properties.

During this project HP approaches for preform preparation were studied with cerium concentrations up to 4%. An evaluation of temperature, pressure, force and time was conducted and presented in Task 1 section.
Previous experiments displayed that ceramic density decayed with increasing levels of cerium concentration, see figure 1.20. Therefore it was necessary to determine the effect of processing variables of the hot press with 4%Ce. Experimental goals included determining the effect of temperature, time and force, upon density and grain size, experimental parameters are outlined in figure 3.1.

Figure 3.1 Experimental HP processing study, constants include material stoichiometry ($Lu_{1.96}Ce_{0.04}SiO_5$) and chamber pressure (~15mtorr).

Run Identification	Temperature (°C)	Dwell Time (minutes)	Applied Pressure (MPa)
LSO 25	1800	300	10
LSO 26	1700	300	10
LSO 27	1600	300	10
LSO 28	1800	60	10
LSO 29	1700	60	10
LSO 30	1600	60	20
LSO 31	1600	60	75

The results of the densification experimental matrix will be discussed in the next few pages.

Increasing time to a five hour dwell at 1600°C and 10 MPa resulted in a dense ceramic (figure 3.2). During the increased dwell period the average matrix grain increased approximately 3.6 times, displayed in figure 3.3.

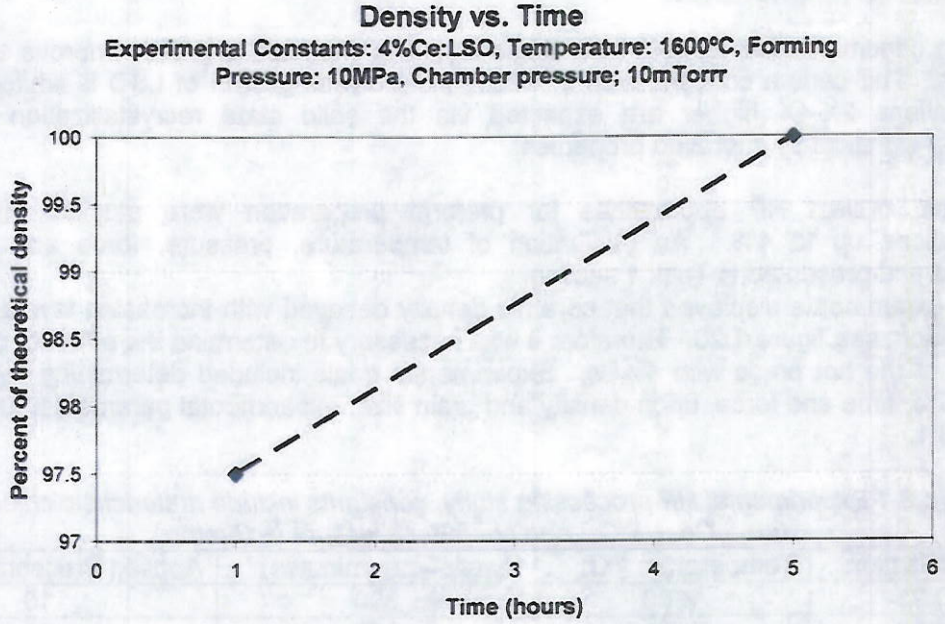

Figure 3.2 Density as a function of time, LSO12 and LSO27 (1600°C, 10 MPa at variable time intervals).

Since there has not yet been a determination on the maximum grain size limit that will inhibit SSR, the general objective is to minimize grain growth by minimizing temperature and time.

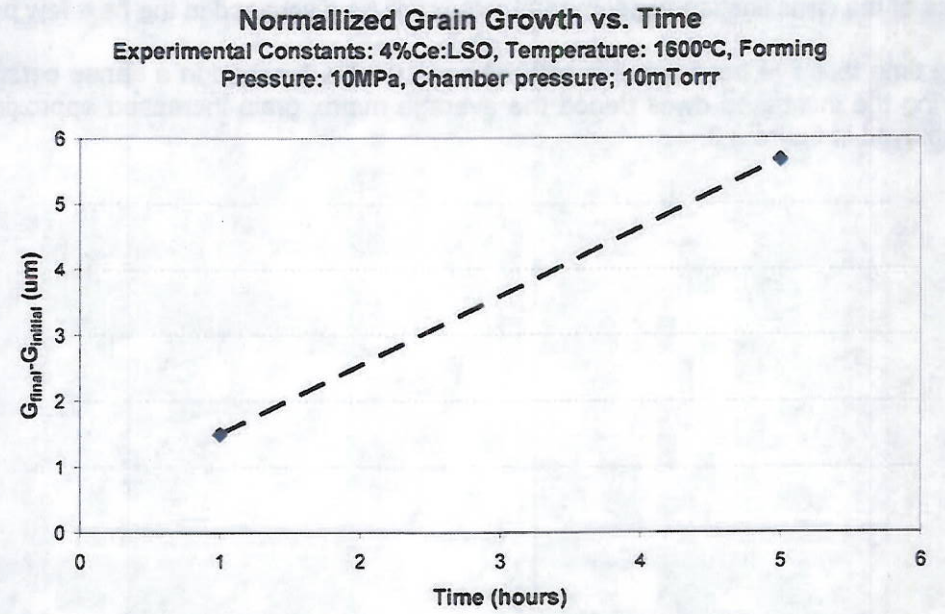

Figure 3.3 Change in grain size as a function of time, LSO12 and LSO27 (1600°C, 10 MPa at variable time intervals). The starting grain size is 1.47μm.

The primary driving force for sintering originates from the reduction of free energy within system and is described as equation 7:

$$\Delta GT = \Delta GV + \Delta Gb + \Delta Gs \qquad \textbf{Eq.7}$$

Where ΔGV, ΔGb, and ΔGs represent the change in free energy associated with volume, boundaries and surfaces of grains. The major thermodynamic driving force for sintering is the reduction in surface area ΔGs, which can be described in equation 8.

$$\Delta Gs = \delta s\, \Delta As \quad \textbf{Eq. 8}$$

Where δsv is surface energy and ΔAs is the change in surface area. Using the relationship between particle curvature and driving force during sintering:

$$\mu a = \mu oa + (P+R\delta sv)\Omega + KT\ln Ca \qquad \textbf{Eq. 9}$$

To full describe the relationship between particle curvature and driving force during hot pressing the applied force is inserted into equation 9. As a result equation 10 contains the mechanism that describes the relationship during hot pressing and that with the addition of force at the same temperature comparable grain size can be achieved with a higher density.

$$\mu a = \mu oa + (Pa+P+R\delta sv)\Omega + KT\ln Ca \quad \textbf{Eq. 10}$$

Where μa is chemical potential, μoa is a reference plane, P is the applied pressure, R is the particle radius, Ω is atomic volume, and Ca is concentration of atoms.

However, experimental results displayed a different characteristic, with the application of additional force when time and temperature was constant. The change in grain growth (ΔG) was less than the ΔG obtained with increasing time by 0.1μm with a 2x increase in pressure, see figure 3.4.

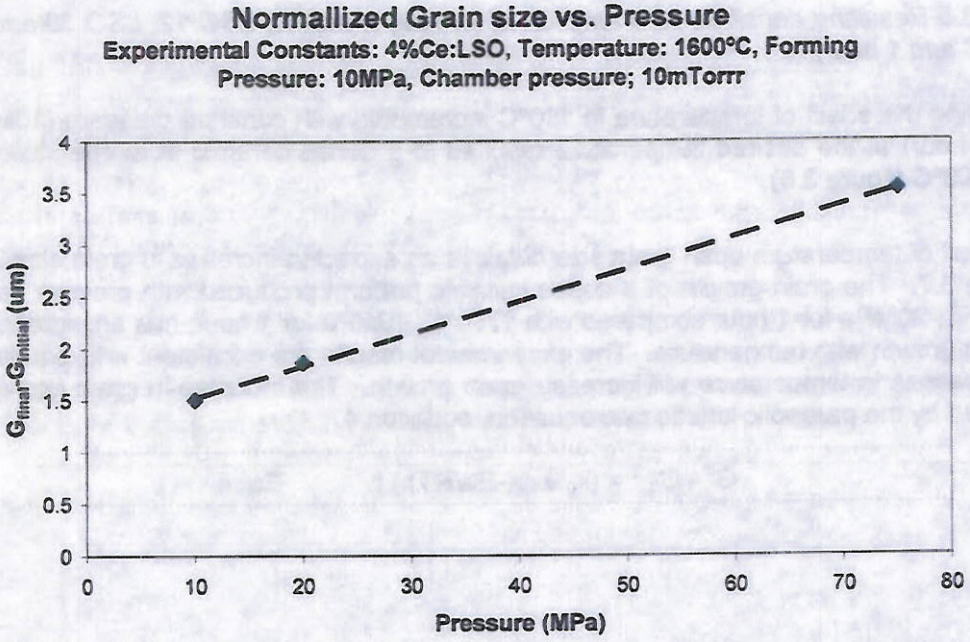

Figure 3.4 Change in grain size as a function of forming pressure, LSO 12, LSO 30 and LSO 31 (1600°C and 1 hour). The initial point source material particle size in not shown, but was 1.02μm.

Consistent with equation 10, an increase in pressure did result in an increase of ceramic density. Two data points were collect at twice and five times the load applied for creating a dense 4% doped LSO ceramic with constants of a one hour dwell at 1600°C, see figure 3.5.

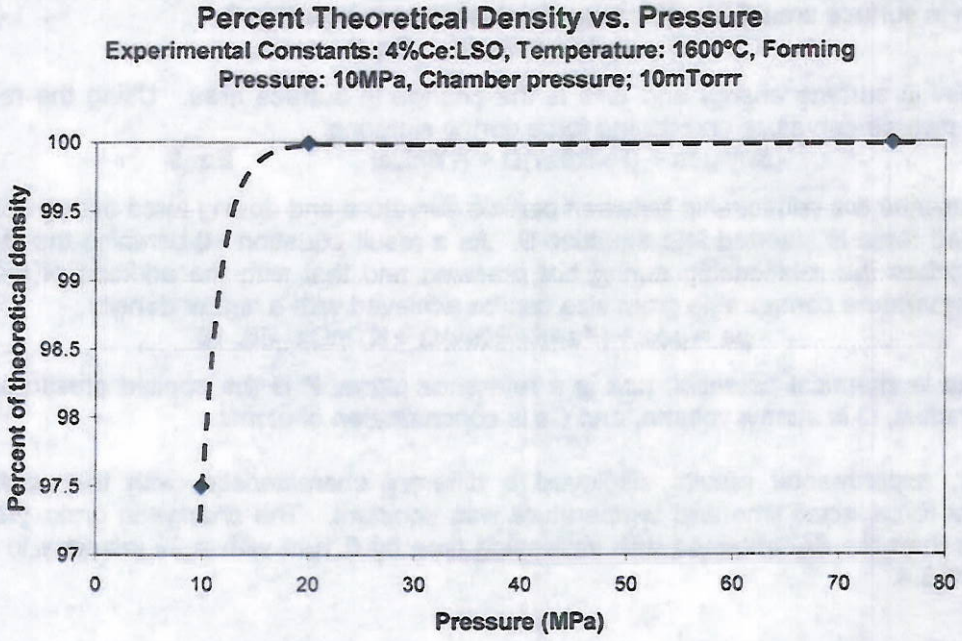

Figure 3.5 Resulting densities as a function of forming pressure, LSO 12, LSO 30 and LSO 31 (1600°C and 1 hour).

Comparing the effect of temperature in 100°C increments with constant pressure (10MPa), and time (1 hour) at the desired temperature resulted in a dense ceramic at temperatures greater than 1700°C (figure 3.6).

The effect of temperature upon grain size displays an expected increase in grain size in located in figure 3.7. The grain growth of a dense ceramic preform produced with process parameters of 1600°C, 20MPa for 1 hour compared with 1700°C, 10MPa for 1 hour, has an increasing effect on grain growth with temperature. The experimental results are consistent with equation 10, in that increases in temperature will increase grain growth. The increase in grain growth can be explained by the parabolic kinetic rate equation, equation 4.

$$G^2 - G_0^{\,2} = (k_0 \exp(-Ea/RT))\, t \qquad \textbf{Eq. 4}$$

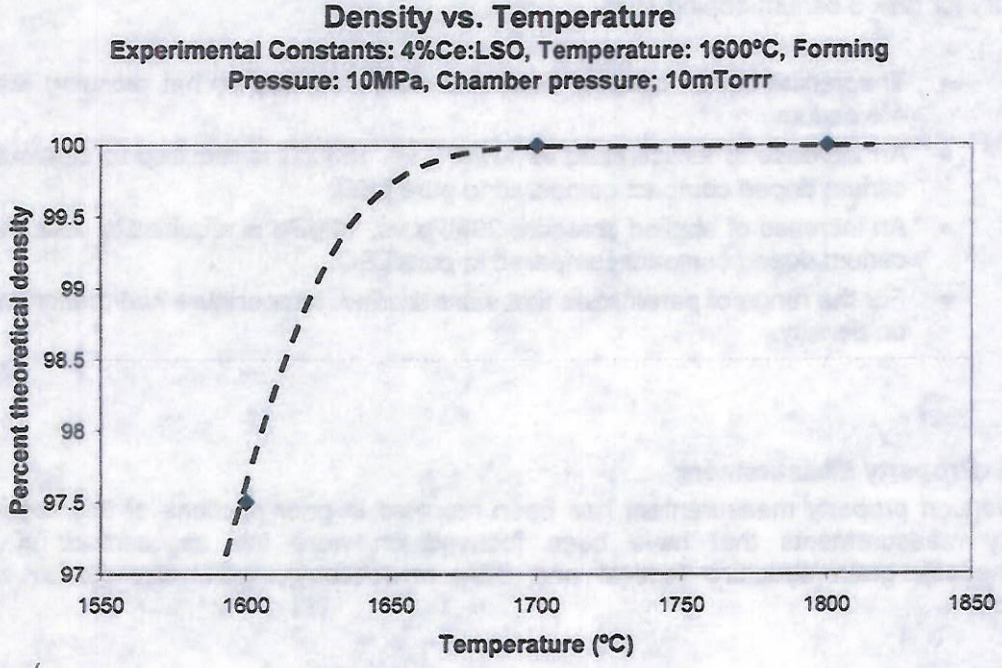

Figure 3.6Resulting densities as a function of forming temperature, LSO 12, LSO 29 and LSO 28 (10 MPa and 1 hour).

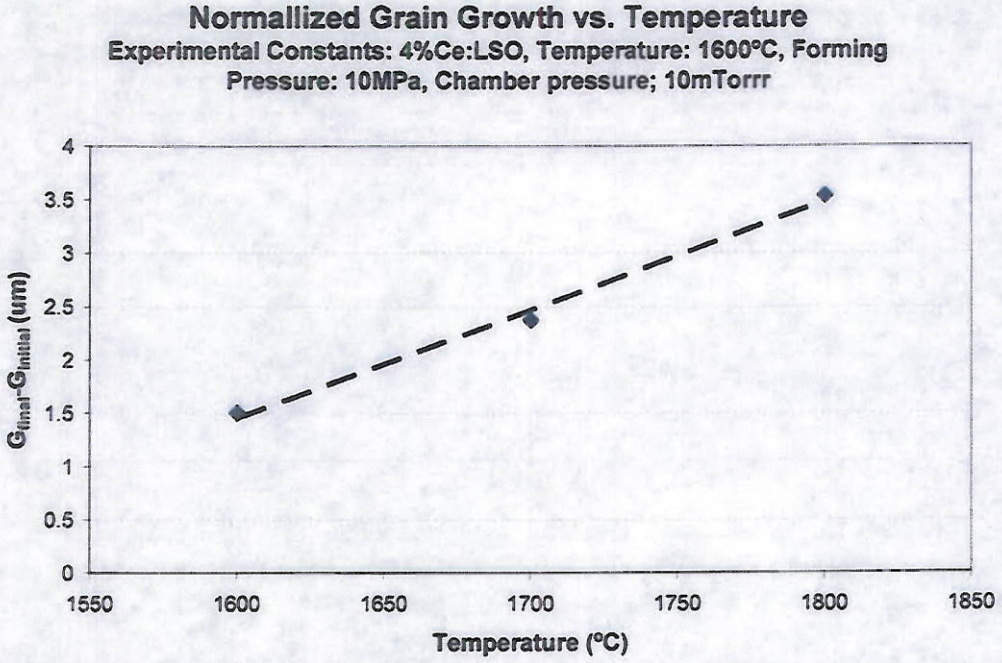

Figure 3.7 Change in grain size as a function of temperature, LSO 12, LSO 29 and LSO 28 (10 MPa and 1 hour). The initial point source material particle size in not shown, but was 1.02µm.

Summary for task 3 cerium doping study:

- Theoretical dense ceramic compacts were obtained by hot pressing with up to 4% cerium
- An increase of temperature to 1700°C vs. 1600°C is required to obtain a dense cerium doped compact compared to pure LSO.
- An increase of applied pressure 20MPa vs. 10MPa is required to obtain a dense cerium doped compact compared to pure LSO.
- For the range of parameters that were studied, temperature had the largest effect on density.

Task 4. Property Measurement

The effort on property measurement has been reported in prior sections of this report. The property measurements that have been focused on were the assessment of density (Archimedes), grain structure (optical and SEM microscopy), grain size (linear intercept method).

Milestones

Task 1:	Demonstration of 96% dense (9 months), 99% density (15 months), 99.9% density (24 months)
	Demonstration of seed attach procedure with >90% coverage (12 months)
Task 2:	Development of Kinetic Rate Model for Primary and Matrix Grains (18 months)
Task 3.	Demonstration of cerium doping (1%-9 months, 2%-18 months, 4%-24 months)
Task 4.	Optical and Scintillator properties (50% of SC – 12 months, 75% of SC-18 months, 90% of SC-24 months) for transmission and light yield.

All milestones, have been met except for optical and scintillation properties in task 4.

Deliverables

Semi-annual Technical Reports (3 total at 6, 12, 18 months after award)
Final Technical Report (1 total at 24 months after award)
Single crystal LSO disks(3 total, 25 mm diameter x 10mm thick, 12 months after award)
Single crystal Ce:LSO disks (3 total, 25 mm diameter x 10mm thick, 1%, 2% and 4% cerium, 24 months after award)

Personnel Supported

This project provides support for the following personnel:

Penn State University EOC:
- Dr. David Snyder - Principal Investigator
- Charles Shanta – MS Graduate Student/Asst. Research Engineer
- Jeremy Potocnak – Research Technician
- Timothy Solomon – Engineering Aid
- Steven Shrawder - Undergraduate Student (Material Science)
- Ryan Hagofsky - Undergraduate Student (Mechanical Engineering Technology)

TRS Technologies, Inc.
- Dr. Wes Hackenburger – Principal Investigator
- Dr. Seongtae Kwon – Research Scientist

Penn State University ARL
- Dr. Tim Eden – Head, Metals and Ceramics Processing
- Chris Wertz – Research Technician

Penn State University Radiation Science and Engineering Center
- Brenden Heidrich-Research Technician

Publications

- Two external presentations are of result of this project.

1. "Solid State Recrystallization of Single Crystal Ce:LSO Scintillator Crystals". Spring Materials Research Society Conference, San Francisco CA, April 2009.

2. "Kinetics of Solid State Recrystallization of Cerium-doped Lutetium Orthosilicate Scintillator Crystal". The 17th American Conference on Crystal Growth and Epitaxy in conjunction with the 14th US Biennial Workshop on Organometallic Vapor Phase Epitaxy.

Interactions/Transitions

a) Participation/presentations at meetings, conferences, seminars:

Two conferences where attended.

1. The Spring Materials Research Society Conference, San Francisco CA, April 2009,
2. The 17th American Conference on Crystal Growth and Epitaxy in conjunction with the 14th US Biennial Workshop on Organometallic Vapor Phase Epitaxy.

b) Consultative and advisory functions to other laboratories and agencies and other DoD laboratories :

No consultative and advisory functions to other laboratories and agencies and other DoD laboratories during this reporting period.

c) Transitions :

- TRS Technologies, Inc. is an industrial partner teamed with Penn State on this project.
- TRS will be responsible for scale up and commercialization of processes for Ce:LSO produced during this program.
- Monthly meetings are held with TRS to present/review technical data from experimental programs, coordinate characterization, and review experimental plans for subsequent months. This approach ensures that TRS is fully integrated into the development process and is monitoring progress of project.
- Material will be made available to DTRA via deliverables for evaluation by outside entities.

New Discoveries, Inventions, or Patent Disclosures

No significant discoveries, inventions, or patent disclosures during this reporting period.

Honors/Awards

No Honors/Awards during this reporting period.

Quad Chart

(See page 51)

SSR Growth of Ce:LSO Scintillator Crystals, David W. Snyder, Penn State University EOC, Grant Number HDTRA1-07-001

Description of Effort: The objective of this project is the development of high resolution, increased sensitivity, low cost cerium-doped single crystal Lutetium-based scintillators ($CeLu_2SiO_5$ (Ce:LSO)) using solid state recrystallization of ceramic LSO. Using the SSR process, the concentration of cerium dopant in LSO can be significantly increased leading to higher scintillation output and lower cost.

Challenges:

-Crack free large area SSR single crystal.

-Seed attachment and optimization of growth kinetics.

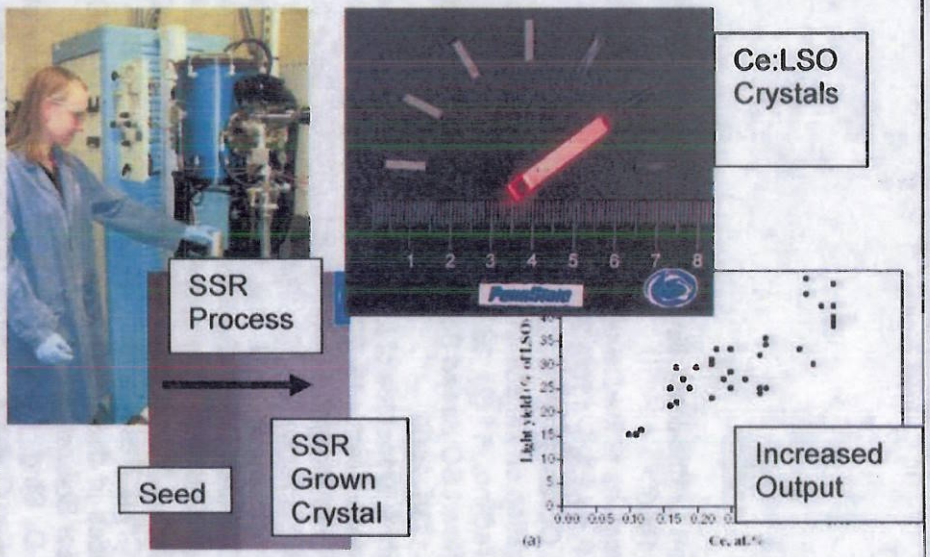

Status of Effort: Determined a predictive crystal growth model for LSO SSR, based on the parabolic rate law. A 3mm x2mm x 3mm Ce:LSO crystal has been produced. Doping LSO with CaO is the key in producing crystals by the SSR method, with a 60x rate improvement over LSO.

Personnel Supported: PI(D.Snyder), MS Graduate Student/Res.Engr.(C.Shanta), two undergraduate students are currently supported.

Publications & Meetings: Two presentations were completed on this project, Spring MRS 2009 and ACCG-17.

Major Goals/Milestones by Project year:

Year 1: Preform densification: 96%, Ce-doping @ 1% seed attach @ >90%, properties @ 50% SC

Year 2: Preform densification: 99%, 99.9%, kinetic rate model, properties @75% SC(18mo), 90% of SC(24mo)

Funding Profile:

Year 1	Year 2	Year 3
11/15/06-10/31/07	11/01/07-07/31/09	
$122.9K	$202.1K	

PI: Dr. David W. Snyder, dsnyder@psu.edu, 724-295-6608, 724-448-5159

References:

[1] C. L. Melcher, "Lutetium Orthosilicate Single Crystal Scintillator Detector", U.S. Patent #4,958,080, Sept. 18, 1990.

[2] A.N. Belsky, *et al.*, "Progress in the Development of $LuAlO_3$-Based Scintillators", *IEEE Trans. Nucl. Sci.*, **48** [4] pp.1095- 1100, 2001.

[3] A.G. Petrosyan, et.al., Optical Materials 24 (1-2): 259-265, 2003.

[4] G. Ren, et al, "Investigation on Defects in Lu2SiO5:Ce Crystals Grown by Czochralski Method", Cryst. Res. Techno., 41 (2), 163-167, 2006.

[5] J.S. Iwanczyk et al., "New LSO Based Scintillators", IEEE Transactions on Nuclear Science, 47 (6), 1781-1786, 2000.

[6] L. Pitol et al., "Scintillation Properties of Lu2Si2O7:Ce3+, a Fast and Efficient Scintillator Crystal", J. Phys.:Condens. Matter 15, 2091-2102 (2003).

[7] D. Pauwels et al., "A Novel Inorganic Scintillator: Lu2Si2O7:Ce3+ (LPS)", IEEE Transactions on Nuclear Science, 47 (6), 1787-1790, 2000.

[8] C.L. Melcher and J.S. Schweitzer, Nucl. Inst. Meth. Phys. Res. A 314, 212, 1992.

[9] S.A. Speakman, W. D. Porter, M. A. Spurrier, C.L. Melcher, " Thermal Expansion and Stability of Cerium-Doped Lu2SiO5" Material Research Bulletin **41** 423-435 (2006)

[10] G. Ren, L. Qui, H. Li, S. Lu, "Investigation on defects in Lu2SiO5:Ce Crystals Grown by Czochralski Method", Cryst. Res. Technol. **41** [2] 163-167 (2006)

[11] C.L. Mechler, "Advances in the Scintillation Performance of LSO:Ce Single Crystals", Transactions on Nuclear Science **50** [4] 762-766 (2003)

[12] L. Qui, H. Li, S. Lu, D. Ding, G. Ren, "Growth and Characteristics of LYSO ($Lu_{2(1-x-y)}Y_{2x}SiO_5:Ce_y$) Scintillation Crystals", Journal of Crystal Growth **281** [2-4] 518-524 (2005)

[13] H. Li, X. Lui, L. Huang, "Fabrication of Transparent Cerium-Doped Lutetium Aluminum Garnet (LuAG:Ce) Ceramics by a Solid-State Reaction Method", J. Am. Cera. Soc. **88** [11] 3226-3228 (2005)

[14] C. Yan, G. Zhao, Y. Hang, L. Zhang, J. Xu, "Czochralski Growth and Crystal Structure of Cerium-Doped Lu2Si2O7 Scintillator", Materials Letters **60** 1960-1963 (2006)

[15] J.S. Reed, Forming Processes, Chapter 20 in *Introduction to the Principles of Ceramic Processing*, John Wiley & Sons, NY, 1988

Addendum: TRS Technologies Final Technical Report

TRS Technologies

Wesley Hackenberger, Ph.D.
TRS Technologies, Inc.
2820 East College Avenue
State College, PA 16801
(814) 238-7485 (Phone)
(814) 238-7539 (FAX)
wes@trstechnologies.com

Final Technical Report for Solid State Recrystallization of Ce:LSO

April 7, 2009
Final Program Status Report: ☒ Yes ☐ No

Prepared Under
Subcontract No. 0001-SA-20116-0209

Name of Contractor:
TRS Technologies, Inc.

Principal Investigator:
Dr. Wesley Hackenberger

Business Address:
2820 East College Avenue

Phone Number:
(814) 238-7485 ext)224

Effective Date of Contract:
November 8, 2007 **Contractor's Monthly Technical Report**

Contract Expiration Date:
October 8, 2008 **Reporting Period:** Nov 8 2007, through April 7, 2009

TRS Technologies

Wesley Hackenberger, Ph.D.
TRS Technologies, Inc.
2820 East College Avenue
State College, PA 16801
(814) 238-7485 (Phone)
(814) 238-7539 (FAX)
wes@trstechnologies.com

A. LSO

LSO powder has been delivered to EOC for various hot pressing experiments.

B. LuAG

The collaboration with EOC on LuAG system showed that optically transparent LuAG ceramics can be obtained by sintering using fine starting powder. The scintillating property of the ceramics was not compatible with single crystal. It was believed that the second phase and processing defect present in the ceramics despite of their apparent transparency are responsible for the low scintillating property. In an effort to remove the processing defects in the sintered ceramics, pressed samples were prepared using calcined powders and also reactive powder was hot pressed. The densities of the sintered and hot pressed samples are listed in the Table I.

Table I Densities of sintered and hot pressed LuAG ceramics

Powder Batch	Calcination	Sintering/HP	Temperature	Time	Density
RB 0706	600°C	Sintering	1800°C	10hr	6.65
RB 0706	500°C	Sintering	1800°C	10hr	6.66
RB 0762	Reactive	Sintering	1800°C	10hr	6.74
RB 0762	Reactive	Hot Pressing	1700°C	1hr	6.72
RB 0762	Reactive	Hot Pressing	1600°C	1hr	6.71
RB 0762	Reactive	Hot Pressing	1500°C	1hr	6.67
RB 0762	Reactive	Hot Pressing	1700°C	5hr	6.72

Hot pressed samples have high density, but they were not transparent. It is believed that carbon from graphite fixtures contaminated samples during hot pressing. The density of hot pressed samples appears to be dependent on the hot pressing condition. The longer time and higher hot pressing temperature resulted in higher density. This implies that all the samples except 1700°C 5hr hot pressed sample were not fully densified and still could have processing defects. The microstructures of hot pressed samples will be investigated along with sintered samples.

Figure 1 shows the polished LuAG ceramics (RB0605 and RB0606) sintered at 1800°C for 10 hrs. Considering the thickness of mounting epoxy for polishing is about 20 mm, the samples have fairly good optical transparency. In Figure 2, polished LuAG samples from calcined and reactive powder are shown. Samples from calcined powder have relatively large diameter due to less shrinkage compared to the reactive powder samples. They have poor transparency presumably due to the formation of aggregates by calcination. This work needs to be directed to lower calcination temperatures.

Figure 1 Polished LuAG ceramics sintered at 1800°C showing transparency.

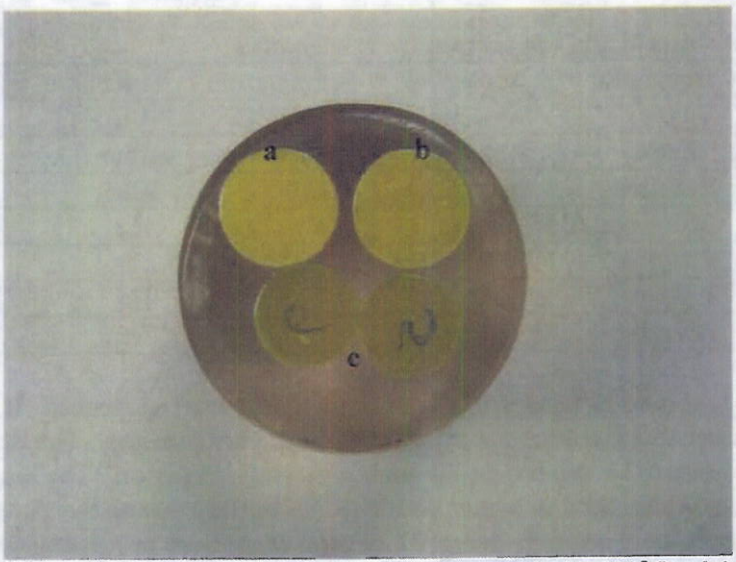

Figure 2 Polished LuAG ceramics from a) 500°C calcined RB0706 b) 600°C calcined RB0706 and c) reactive RB0762. RB0762 samples have number written on the bottom faces showing their transparency.

Microstructure of LuAG

Microstructural observation of LuAG ceramics was conducted. Figure 3 shows the polished microstructure of various samples. It was reported that samples from calcined powder were not transparent. It is shown that the reason for the poor transparency of calcined powder samples is not the residual pores. The white spots observed in x200 pictures are presumably second phase or inhomogeneous grain boundary, which are believed to be responsible for the poor transparency.

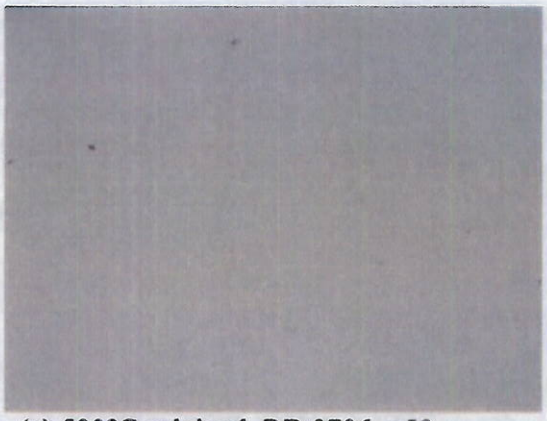

(a) 500°C calcined RB 0706, x50

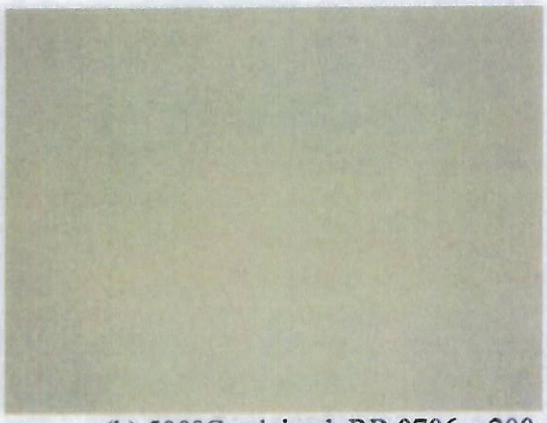

(b) 500°C calcined RB 0706, x200

(c) 600°C calcined RB 0706, x50

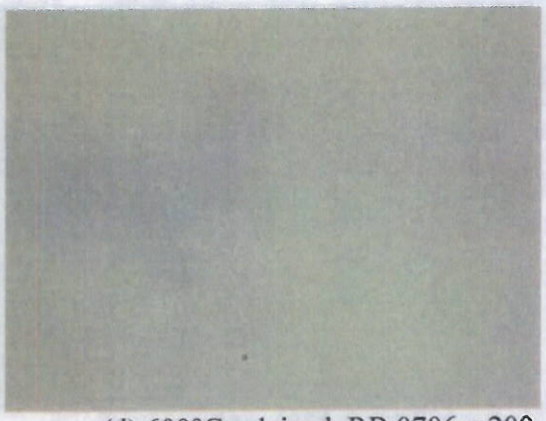

(d) 600°C calcined RB 0706, x200

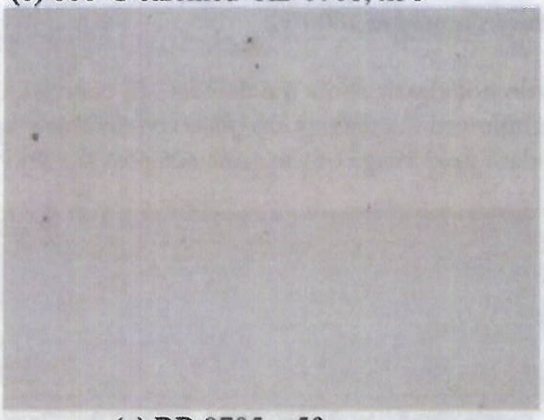

(e) RB 0705, x50

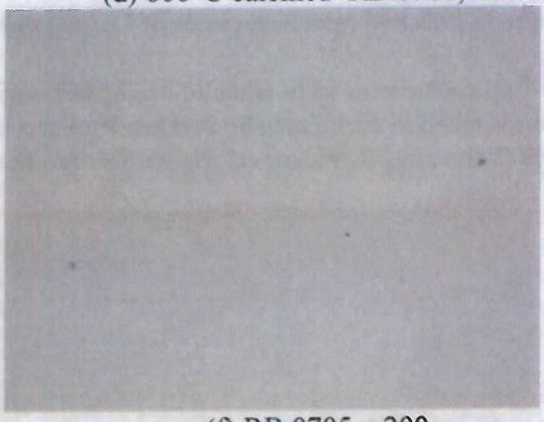

(f) RB 0705, x200

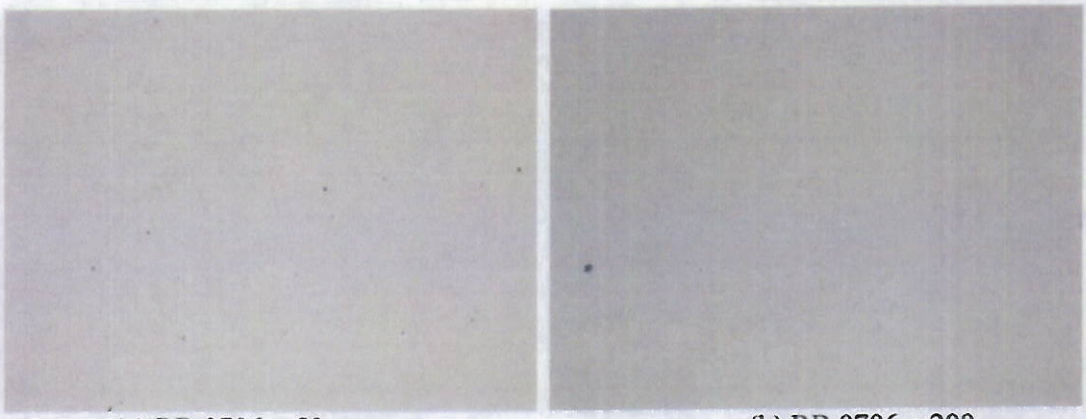

(g) RB 0706, x50 (h) RB 0706, x200

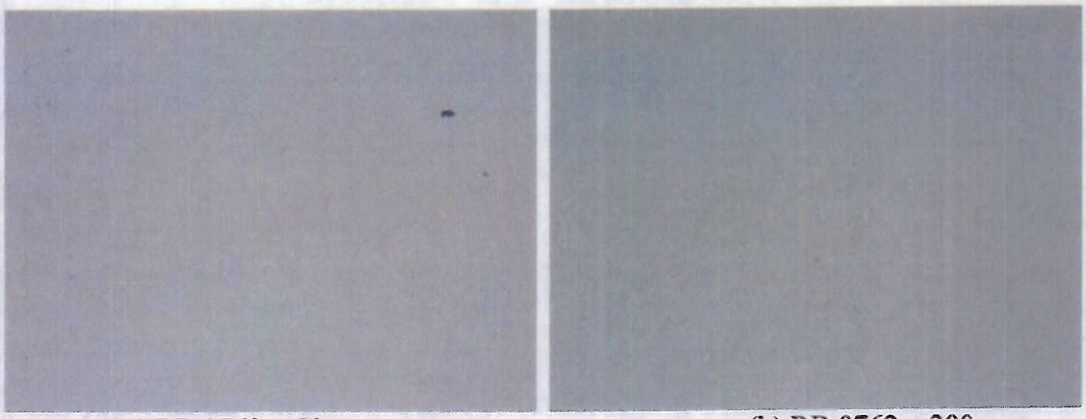

(g) RB 0762, x50 (h) RB 0762, x200

Figure 3. Polished microstructures of LuAG ceramics sintered at 1800°C.

The microstructures were taken in bright field and do not clearly show the defects. In contrast, the pictures taken in dark field showed inside of the sample and the defects are observed cumulatively through the sample thickness. Figure 4 shows the dark field image of the same samples shown in the Figure 1.

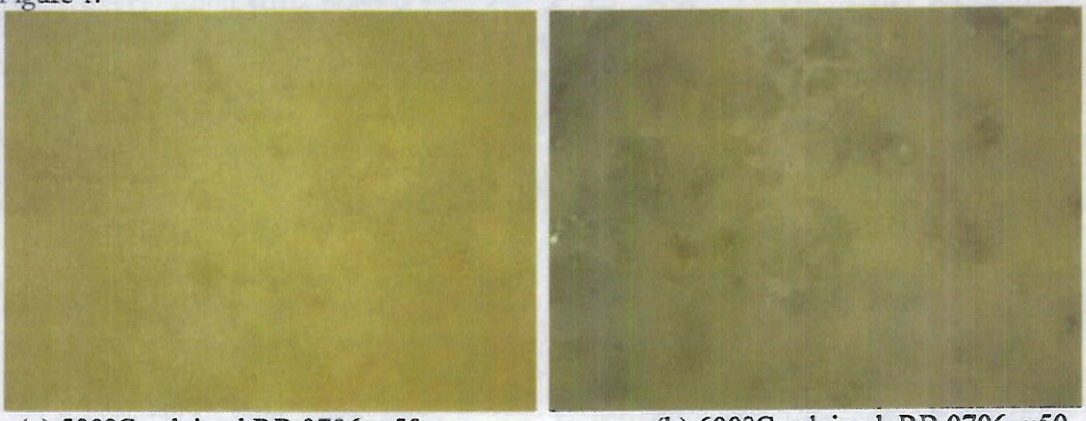

(a) 500°C calcined RB 0706, x50 (b) 600°C calcined RB 0706, x50

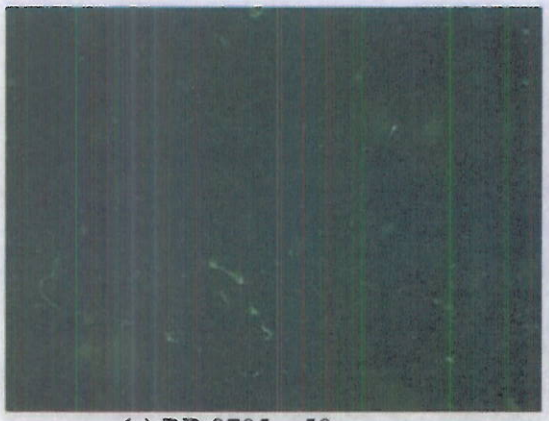

(c) RB 0705, x50

(d) RB 0705, x50

(e) RB 0762, x50

Figure 4. Dark field images of polished LuAG ceramics sintered at 1800°C.

planned

It is apparent that even though some samples are optically transparent (c, d and e), there are many defects inside the samples, which are believed to be critical for the scintillation property. Calcination was planed as one of the way to remove the processing defects by removing organic contaminants, but resulted in causing another problem. The other approach to remove the processing pores was hot pressing. Figure 5 illustrates the polished microstructure of hot pressed LuAG samples. The porosity corresponds well to the measured density reported previously. The sample hot pressed at 1700°C for 5 hr appears to be very dense. The samples will be annealed in air in an effort to remove the carbon and recover the transparency.

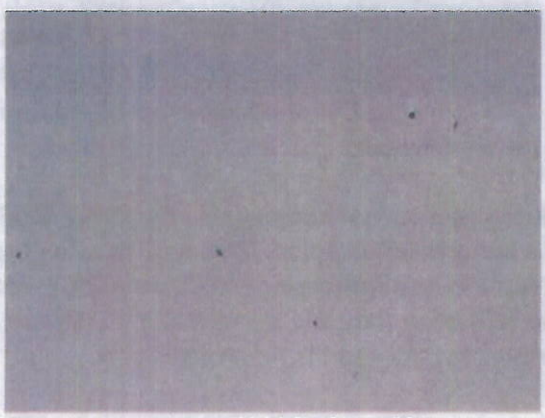

(a) Hot pressed No1, 1700°C 1hr, x50

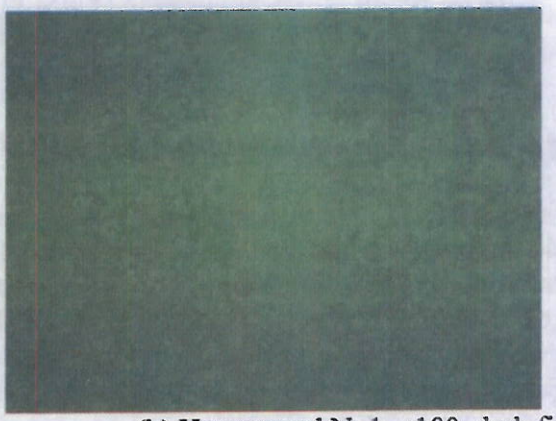

(b) Hot pressed No1, x100, dark field

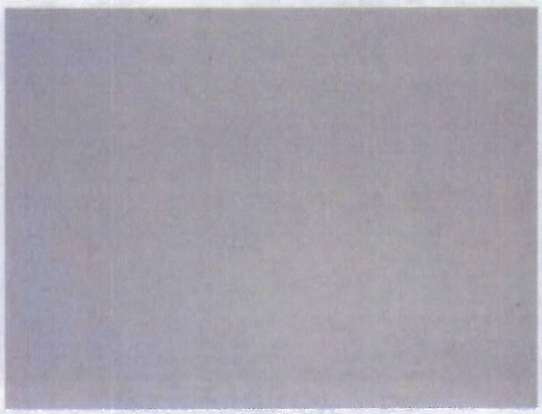

(c) Hot pressed No2, 1600°C 1hr, x50

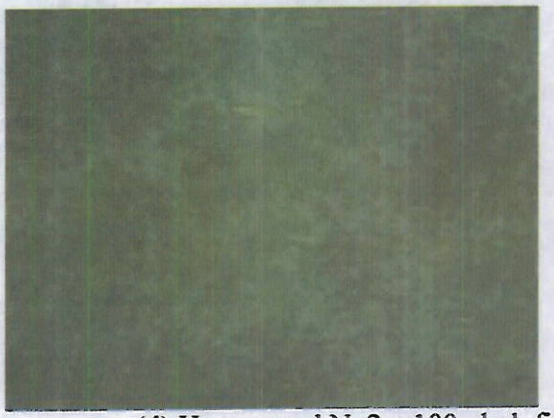

(d) Hot pressed No2, x100, dark field

(e) Hot pressed No3, 1500°C 1hr, x50

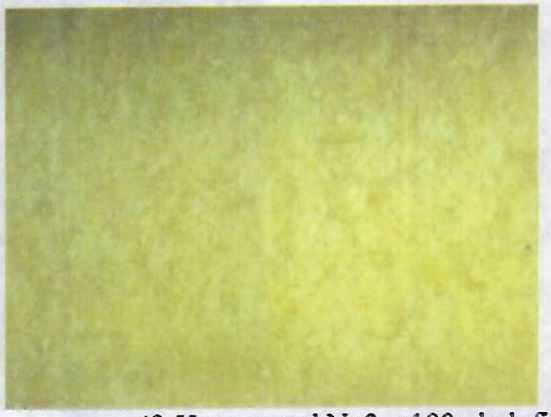

(f) Hot pressed No3, x100, dark field

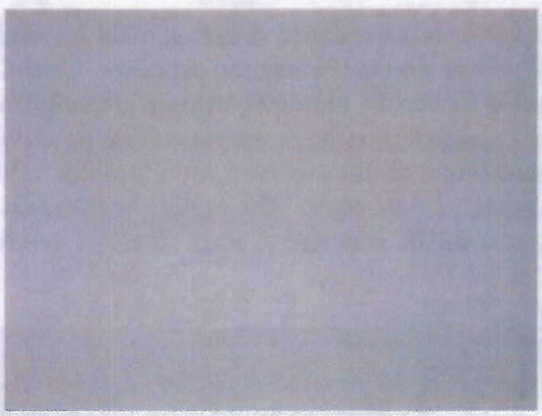

(g) Hot pressed No4, 1700°C 5hr, x50

(h) Hot pressed No4, x100, dark field

Figure 5. Polished microstructures of hot pressed LuAG ceramics.

It is shown that bright field images are very good except the sample hot pressed at 1500°C. Dark field images show that there are still defects in the hot pressed samples. It should be also noted that the defects in 1700°C hot pressed sample appears to be aligned perpendicular to the pressure direction during hot pressing (Figure 5 (h)). After removing the carbon and making the sample more transparent the observation of remaining defects in dark field is believed to give information on the research direction.

LuAG ceramics with bare eyes contained significant amount of defects in microscopic observation. The most of the defects had fabric related appearance. The attempt to remove the defects by using calcined powder resulted in unsuccessful due to the poor deformability of calcined powder during pressing. The optical transmittance of the polished samples were measured using spectrophotometer (Beckman Coulter, DU800) located in PSU (Prof. Vogler). Figure 6 shows the transmittance result of RB705 and RB706 samples.

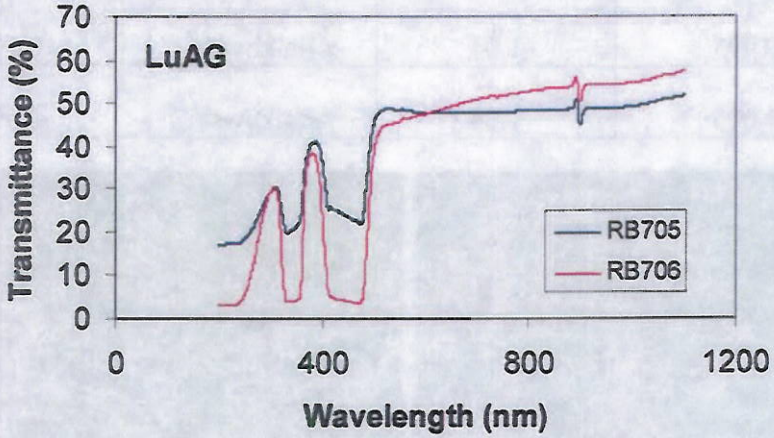

Figure 6 Transmittance result of polished LuAG ceramics sintered at 1800°C, the optical view of the samples are shown in Figure 1.

It is shown that 50~60% transmittance is achieved at the wave length above 500nm. The reason for RB705 has higher transmittance at lower wavelength is believed due to the fact that diameter of the samples were not large enough to cover the entire slot for the measurement at caused leakage of the light. RB706 sample showed close to zero base line indicating better fitting of the sample to the apparatus. The appearance of the samples was shown in Figure 1.

As a continuation of using calcined powder approach to remove the processing defect in sintered ceramic, it will be attempted to conduct CIP after heating uniaxially pressed sample. Uniaxial press will be conducted at very low pressure, ~10MPa and the heating will be conducted to 400°C to remove the organic contamination. Cold isostatic pressing (CIP) will be conducted to increase the green density after heating. The heating temperature is designed to prevent any possible neck formation of powder to realize of high pressure during CIP to produce homogeneous, high-density green body.

Calcined LuAG powder resulted in low sintered density due to poor deformation of granules during pressing. The main reason for using calcined powder is to remove organic contaminations resulting in fabric-shaped defects in the sintered body. As a continuation of using calcined powder approach to remove the processing defect in sintered ceramic, it was attempted to conduct CIP after heating uniaxially pressed sample. Uniaxial press was conducted at very low pressure, ~10MPa and the heating was conducted to 400°C to remove the organic contamination. Cold isostatic pressing (CIP) was conducted to increase the green density after heating. The heating temperature was designed to prevent any possible neck formation of powder to realize of high pressure during CIP to produce homogeneous, high-density green body. Samples were sintered at 1800°C for 10 hr in the vacuum, the same condition as most of the sintering runs. Table I summaries the powder batch used for the pressing, calcination, CIP experiment.

Figure 7 shows the optical microstructures of sintered samples in comparison with previously process samples. It should be noted that there was a remarkable progress in removing

defects in the sintered ceramics. When we consider that the samples shown in the Figure 7 (c) and (d) are also optically transparent with bare eyes as shown in the Figure 1, we can expect much higher transparency with samples calcined after pressing and subsequently CIP samples even though optical appearances are similar.

Table II Summary of the LuAG powder batches used for pressing, calcination, CIP experiment

Batch	Al_2O_3 Stoichiometry	γ-Al_2O_3 LOI	Al_2O_3 Spec.	tetraethyl orthosilicate
RB 0705	0.995	1.04	γ-Baikowski	0.5%
RB 0706	1.005	1.04	γ-Baikowski	0.5%

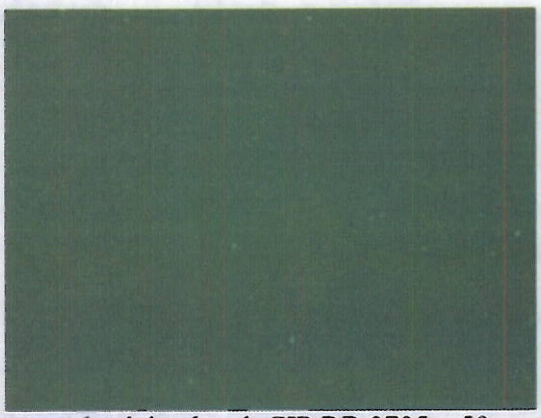

(a) pressed calcined and CIP RB 0705, x50

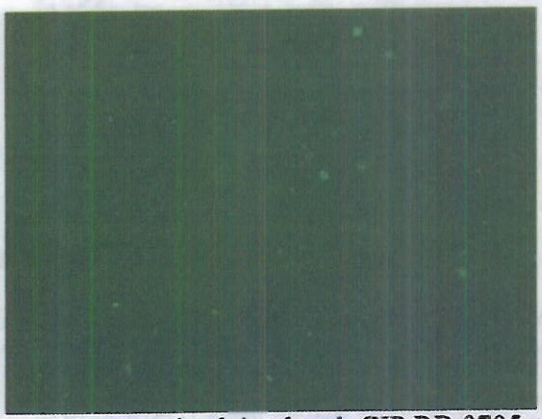

(b) pressed calcined and CIP RB 0705, x50

(c) RB 0705, x50

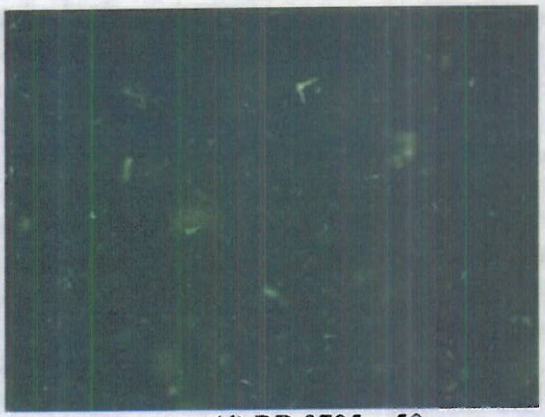

(d) RB 0705, x50

Figure 7 Dark field optical microstructure of RB0705 and RB0706 samples.

The transmittance result of sample 5 from improved method is shown in Figure 8 in comparison with previously reported normally processed RB 0705 and RB0706 samples. The higher transmittance in high wave length region might be due to light leakage, but the current sample

with improved process shows higher transmittance than previous process samples at wavelength below 400nm as well.

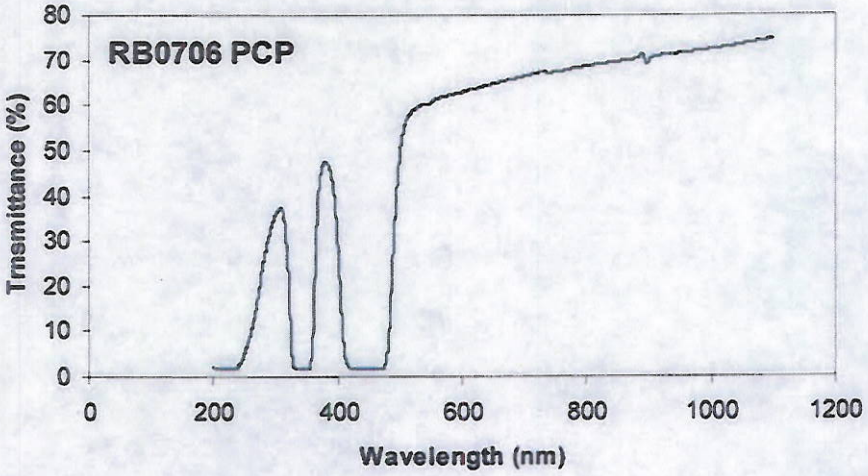

(a)

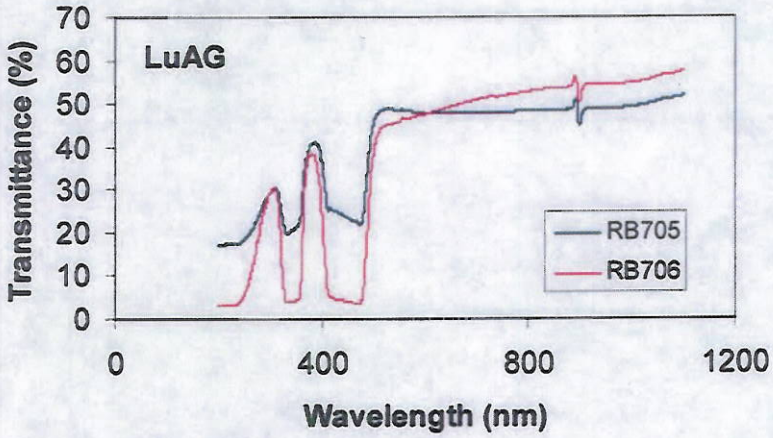

(b)

Figure 8 Transmittance result of polished LuAG ceramics sintered at 1800°C (a) RB0706 process in improved method, press calcine CIP and (b) conventional method

DEPARTMENT OF DEFENSE

DEFENSE TECHNICAL
INFORMATION CENTER
8725 JOHN J. KINGMAN ROAD,
SUITE 0944
FT. BELVOIR, VA 22060-6201
ATTN: DTIC/OCA

DEPARTMENT OF DEFENSE CONTRACTORS

EXELIS, Inc.
1680 TEXAS STREET, SE
KIRTLAND AFB, NM 87117-5669
ATTN: DTRIAC